AGU PUBLICATIONS

JGR

Journal of Geophysical Research: Atmospheres

RESEARCH ARTICLE
10.1002/2017JD026598

Key Points:
- In the Northern Hemisphere (108 km model resolution), aircraft emissions contribute ~1.3% and 0.2% of total O_3 and $PM_{2.5}$ at surface
- Incorporating full-flight aircraft emissions at a fine resolution reduced model bias by up to ~5-11% for NO_2 in UTLS region
- The 108 km resolution showed ~70 times and ~13 times higher impacts for O_3 and $PM_{2.5}$ in North America than 36 km due to grid resolution and transport

Supporting Information:
- Supporting Information S1

Correspondence to:
S. Arunachalam,
sarav@email.unc.edu

Citation:
Vennam, L. P., Vizuete, W., Talgo, K., Omary, M., Binkowski, F. S., Xing, J., … Arunachalam, S. (2017). Modeled full-flight aircraft emissions impacts on air quality and their sensitivity to grid resolution. *Journal of Geophysical Research: Atmospheres*, *122*, 13,472–13,494. https://doi.org/10.1002/2017JD026598

Received 3 FEB 2017
Accepted 29 NOV 2017
Accepted article online 7 DEC 2017
Published online 22 DEC 2017

Modeled Full-Flight Aircraft Emissions Impacts on Air Quality and Their Sensitivity to Grid Resolution

L. P. Vennam[1,2], W. Vizuete[2], K. Talgo[1], M. Omary[1], F. S. Binkowski[1], J. Xing[3,4], R. Mathur[3], and S. Arunachalam[1]

[1]Institute for the Environment, University of North Carolina at Chapel Hill, Chapel Hill, NC, USA, [2]Gillings School of Global Public Health, University of North Carolina at Chapel Hill, Chapel Hill, NC, USA, [3]U.S. Environmental Protection Agency, Research Triangle Park, Durham, NC, USA, [4]Now at School of Environment, Tsinghua University, Beijing, China

Abstract Aviation is a unique anthropogenic source with four-dimensional varying emissions, peaking at cruise altitudes (9–12 km). Aircraft emission budgets in the upper troposphere lower stratosphere region and their potential impacts on upper troposphere and surface air quality are not well understood. Our key objective is to use chemical transport models (with prescribed meteorology) to predict aircraft emissions impacts on the troposphere and surface air quality. We quantified the importance of including full-flight intercontinental emissions and increased horizontal grid resolution. The full-flight aviation emissions in the Northern Hemisphere contributed ~1.3% (mean, min–max: 0.46, 0.3–0.5 ppbv) and 0.2% (0.013, 0.004–0.02 μg/m^3) of total O_3 and $PM_{2.5}$ concentrations at the surface, with Europe showing slightly higher impacts (1.9% (O_3 0.69, 0.5–0.85 ppbv) and 0.5% ($PM_{2.5}$ 0.03, 0.01–0.05 μg/m^3)) than North America (NA) and East Asia. We computed seasonal aviation-attributable mass flux vertical profiles and aviation perturbations along isentropic surfaces to quantify the transport of cruise altitude emissions at the hemispheric scale. The comparison of coarse (108 × 108 km^2) and fine (36 × 36 km^2) grid resolutions in NA showed ~70 times and ~13 times higher aviation impacts for O_3 and $PM_{2.5}$ in coarser domain. These differences are mainly due to the inability of the coarse resolution simulation to capture nonlinearities in chemical processes near airport locations and other urban areas. Future global studies quantifying aircraft contributions should consider model resolution and perhaps use finer scales near major aviation source regions.

Plain Language Summary In the Northern hemisphere, aircraft emissions contribute ~1.3 % and 0.2 % of total O_3 and $PM_{2.5}$ concentrations at the surface. Incorporating full-flight aircraft emissions at a fine resolution improved model estimates of NO_2 by ~5–11% when compared to field campaign observations in upper troposphere lower stratosphere region. Coarse resolution showed ~70 times and ~13 times higher aviation impacts for O_3 and $PM_{2.5}$ when compared to fine resolution over North America. We attribute these overestimates to physical and chemical processes in the choice of grid resolution, as well as due to intercontinental transport of pollution.

1. Introduction

In the atmospheric and air quality community, we have good understanding of the chemical and physical processes occurring in the free troposphere and stratosphere. Only limited knowledge is available, however, concerning the chemistry and transport of pollutants at the boundary of the upper troposphere and lower stratosphere (UTLS) (Finlayson-Pitts & Pitts Jr, 2000). The physical and chemical properties of the UTLS and mid-troposphere are different than the surface, and pollutants found there have the potential for a global intercontinental impact on surface air quality. For example, oxides of nitrogen (NO_x = NO + NO_2) have a lifetime of 1–2 weeks in the UTLS, compared with just a few hours in the boundary layer (Jaegle, 2007). Thus, UTLS pollutants are subject to intercontinental transport (Stohl et al., 2002) due to strong winds and synoptic flow (Holloway et al., 2003). Recently, increased focus has been devoted to study intercontinental transport (Leibensperger et al., 2011; Reidmiller et al., 2009), its impact on human mortality (Anenberg et al., 2009; West et al., 2009), and the interaction of UTLS with the troposphere (Jacob et al., 1999; Jaffe et al., 1999; Lin et al., 2000, 2014). Yet model predictions disagree (Henderson et al., 2011; Zyryanov et al., 2012) with observations in the upper troposphere region. Studies (Allen et al., 2012) have highlighted the lack of UTLS emission sources in regional

and some global models leading to uncertainties in model predictions. One important and less studied emission source is aviation. This rapidly growing transportation sector is a critical anthropogenic emission source in the upper troposphere. An early comprehensive Intergovernmental Panel for Climate Change report (Penner et al., 1999) discussed aviation impacts on the atmosphere both in past (1999) and future (2050) years. It emphasized that the NO_x emissions in the UTLS increased O_3 concentrations by 6% in 1999 and may increase O_3 by 13% in 2050. This report highlighted that the key areas of scientific uncertainty such as the role of NO_x on O_3 concentrations and transport of aviation emissions in UTLS region limit their ability to project aircraft impacts on atmosphere. Globally 92.5% of aviation fuel is burned in the Northern Hemisphere and 74.6% of it is burned at cruise altitudes (Olsen et al., 2013; Wilkerson et al., 2010) near the UTLS region.

Though aviation contributes only ~3% of total anthropogenic NO_x emissions (Wauben et al., 1997), the majority is directly released in UTLS and their surface impacts can be high due to intercontinental transport followed by subsidence (Leibensperger et al., 2011). Few studies have attempted to quantify the contribution of this pollution source on UTLS and surface air quality. An early study (Beck et al., 1992) used a two-dimensional longitude versus height model to assess the impact of civil aircraft emissions and found that aircraft emissions can increase NO_x concentrations by 40% (20 parts per trillion by volume (pptv)) and O_3 by 16% (8–10 ppbv) near cruise altitudes (9–12 km). Later studies (Gauss et al., 2006; Kentarchos & Roelofs, 2002; Wauben et al., 1997) using a 3-D chemistry transport model saw slightly higher perturbations. Gauss et al. (2006) predicted that near the tropopause aircraft emissions increased zonal (30–60 N) mean odd reactive nitrogen (NO_y = NO_x + PAN + HNO_3 + other nitrogen containing species) by 156–322 pptv and O_3 mixing ratios by 3.1–7.7 ppbv depending on season in the Northern Hemisphere. Kohler et al. (2008) investigated the sensitivity of atmospheric composition to aircraft NO_x emissions as a function of location, altitude, and emission perturbation magnitude. The authors emphasized that the aviation NO_x emissions at altitudes of 11–15 km play a crucial role in changing O_3 concentrations and predicted a 6 ppbv maximum increase in zonal annual mean O_3. These early studies predominantly focused on ozone and NO_x perturbations due to aviation emissions in the upper troposphere. These studies, however, relied on global models with coarse resolution (such as 5.6° × 5.6°) and used older emission inventories such as Baughcum et al. (1998), AERO2k, and Abatement of Nuisance Caused by Air Traffic/European Commission (Gardner et al., 1997). These inventories can differ in spatial and temporal resolution when compared with the most recent emission inventories developed by the Aviation Environmental Design Tool (AEDT) (Wilkerson et al., 2010). The AEDT has greater utilization of actual radar tracking and highly resolved emissions distribution (Olsen et al., 2013). Therefore, assessing aviation perturbations with more recent emission inventories and updated models is important to improve scientific understanding of aviation environmental impacts, especially with increasing growth in aviation sector.

In recent years, studies related to surface air quality impacts of full-flight aircraft emissions including both Landing and Takeoff emissions (LTO, emissions occurring $<$1 km) and cruise altitude aviation emissions (CAAE, emissions occurring $>$1 km) have increased due to their potential impact on human health. This major concern arose as Barrett et al. (2010) predicted globally ~8,000 premature mortality attributable to cruise altitude emissions, which motivated researchers to understand the chemical and physical processes responsible for surface impacts associated with cruise emissions. A tracer-based study with no chemistry and only transport and wet deposition processes (Whitt et al., 2011) using the GATOR-GCMOM model (Jacobson et al., 2011) was conducted to study the transport of cruise emissions. This study found that the timescale for vertical mixing is longer than the lifetime of the tracer and emphasized that the surface air quality is unlikely to be affected from cruise emissions solely due to transport. Later, Lee et al. (2013) approached this question differently and relied on predictions from the full chemistry transport CAM-Chem model (Lamarque et al., 2012) and found that aviation-induced perturbations of O_3 and NO_y are less than 1 ppb near the surface. In addition, they mentioned that these perturbations should have negligible effect on the surface air quality when compared with other anthropogenic source impacts and also showed that ground-level aviation impacts from cruise-level emissions are higher than LTO emissions. These results are further supported by Jacobson et al. (2013), who used a one-way nesting chemistry transport model with subgrid scale treatment and found that aircraft emissions increased O_3, PAN, and temperature near the surface by ~0.4%, ~0.1%, ~0.01 K and in the upper troposphere by ~ 2.5%, ~5% and ~0.03 K.

These prior aviation-related studies utilized global model operating on relatively coarse horizontal resolutions of 4° × 5° (Barrett et al., 2010), 4° × 5° (Jacobson et al., 2011, 2013), and 2° × 2.5° (Lee et al., 2013).

Recent studies (Ma et al., 2014, 2015) found that finer horizontal resolution in global models can improve physical and chemical interactions (such as aerosol-cloud interactions) in model predictions and also reduced low biases (by a factor of 5) for aerosol predictions (like black carbon) near the surface. The authors also stated that finer resolution model predictions agree better with observations. Additionally, these global models (Yan et al., 2016) can underrepresent some of the nonlinearities in O_3 changes, emissions contrasts between urban and rural locations, and vertical transport due to coarser resolution. To address these differences in scale, researchers have recently quantified aviation impacts using a combination of global, regional, and dispersion models (Yim et al., 2015). Their results provided region-based aviation-attributable population exposure and concluded that 23% of airports showed higher near-field population exposure to aviation-attributable $PM_{2.5}$ than global average exposure. The authors also indicated that by including a different nested regional model in a global model, the aviation-attributable ground level O_3 increased by 12% and $PM_{2.5}$ decreased by 29%. Nevertheless, there are several limitations in the implementation of this compilation of different modeling systems. For example, there are differences in chemical mechanisms and transport schemes among the different models that would influence aviation contributions resulting in an inconsistency when trying to make a regional versus global comparison.

The assessment of aircraft emissions on air quality could be improved with emission inventories that include full-flight profiles and computationally efficient application of a finer spatial resolution modeling. In this study we investigate the impact of full-flight emissions on surface air quality at hemispheric and regional levels. Here the Community Multi-scale Air Quality (CMAQ) model with a domain covering the entire Northern Hemisphere (Mathur et al., 2012, 2017) at a horizontal grid cell resolution of 108 × 108 km^2 is used to study the aviation impact. This hemispheric model is ~2–4 times finer than the typical horizontal resolution (4° × 5°, 2° × 2.5°) used in prior global model studies. Additionally, having a finer vertical resolution is particularly crucial for investigating the impact of an emission source-like aviation in the upper troposphere/tropopause region. Thus, in this study, we further refined the model vertical structure to have finer resolution (~ 44 layers) than the traditional model vertical resolutions (~ 17 and ~ 34 layers, coarser vertical resolution) typically used in most of the regional modeling applications (Appel et al., 2011, 2017). Here in this study in addition to the overall hemispheric aviation-attributable perturbations we closely examined the impacts in three major subregions (North America (NA), Europe (EU), and East Asia (EA)) that have relatively higher aviation emissions. We also studied the aviation-attributable perturbations using mass flux vertical profiles and cross-sectional isentropic analysis to understand the vertical transport of aviation emissions. In addition to hemispheric modeling, we also performed regional-scale modeling utilizing a 36 × 36 km^2 continental U.S. scale to compare the differences in aviation-attributable impacts for different model resolutions. Overall, this framework may help reduce uncertainties in model predictions and provide an improved understanding of physical and chemical changes occurring in the upper atmosphere due to aviation and its impacts on surface air quality.

2. Methodology

2.1. Air Quality Modeling

We used the CMAQv5.0.2 model (Byun & Schere, 2006) with updated CB05 condensed toluene gas phase mechanism (Sarwar et al., 2011; Whitten et al., 2010) and AERO6 aerosol module to carry out both regional- and hemispheric-scale modeling and to assess air quality impacts of aircraft emissions. We used Weather Research and Forecasting model (WRFv3.6.1) (Skamarock et al., 2008) to downscale NASA's Modern-Era Retrospective Reanalysis (MERRA) (Rienecker et al., 2011) inputs to produce meteorological input data for CMAQ. MERRA is a global reanalysis data set that assimilates observations and satellite products and has a horizontal grid resolution of 0.5° × 0.67° with 72 vertical levels extending to 0.01 hPa. We initialized WRF at 0000 UTC 1 January 2004 and ran continuously through 0000 UTC 1 January 2006 using MERRA data. The first 12 months of the simulation (1 January to 31 December 2004) were used as a spin-up period for the WRF model. We ran 12 months spin-up only for the meteorological model (WRF). Our initialization data set (MERRA) does not have soil temperature and moisture fields to initialize WRF, so we have to process those fields from an alternate source; in this case the Global Forecast System. The longer spin-up is to allow for the soil and atmosphere fields to come into equilibrium since they are coming from different sources. Further, to better represent the upper troposphere dynamics and hemispheric transport, the model needs a relatively long time to stabilize. We thus decided to do an annual spin-up to avoid any initialization

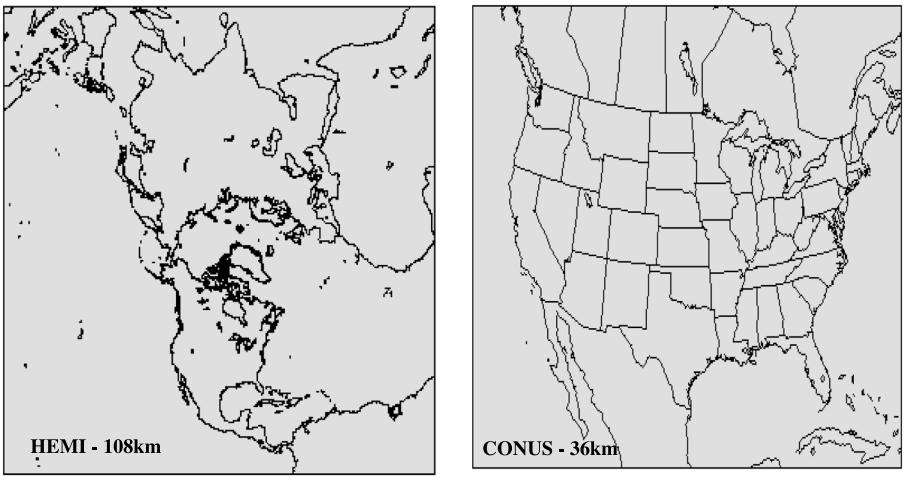

Figure 1. Modeling domains (left) (HEMI) at 108 km and (right) (CONUS) at 36 km horizontal resolutions.

uncertainties. The domain configurations (Table S1 in the supporting information), model vertical structure (Table S2), and physical options (Table S3) used in WRF are included in supporting information. Table S4 shows an evaluation of WRF model output with observations. The model bias and error for this model configuration and time period are similar to those found in benchmark simulations and previous studies (Xing et al., 2015). We ran WRF over two stand-alone domains: (1) 108 × 108 km^2 (hereafter denoted as 108 km) northern hemispheric (HEMI, (−15°S to 90°N, −179°W to 179°E)) with a polar stereographic projection and (2) 36 × 36 km^2 (hereafter denoted as 36 km) Contiguous United States (CONUS, (18.3°N to 57.0°N, −136.9°W to −58.8°W)) with a Lambert conformal projection, as shown in Figure 1. The CMAQ northern hemispheric application (HEMI) is a newer platform with 108 km horizontal resolution that has been used in recent studies (Mathur et al., 2017; Sarwar et al., 2014; Xing et al., 2015), and this is the first study to use that application for studying the impacts of aircraft emissions. For the CONUS application, we used a traditional North American domain at a 36 km horizontal resolution. We also used consistent meteorology (from MERRA) for both the hemispheric and regional scales, and drove the regional-scale application using downscaled boundary conditions from the hemispheric model.

For regional domains, incorporating dynamically and chemically downscaled boundary conditions from global models is important given the increased role of hemispheric transport on regional studies (Lin et al., 2000, 2014). Earlier studies (Henderson et al., 2014; Lam & Fu, 2009) showed higher ozone mixing ratios in the upper regional model layers when downscaled from global models and discussed the vertical incompatibility between regional and global models. Here we use the CMAQ model for an application over HEMI with identical physical and chemical model processes to generate boundary conditions for the CONUS domain. By doing this, we are able to maintain consistency in the chemical mechanisms and dynamics for the boundary conditions in the regional domain.

The CMAQ model configurations and data used for two domains are in Table 1. We used the National Emissions Inventory (NEIv4.3) for the year 2005 (U.S. Environmental Protection Agency, 2007) and the Sparse Matrix Operator Kernel Emissions (SMOKE) SMOKE model (Houyoux et al., 2000) to generate gridded emissions for all anthropogenic sources except aviation for the CONUS domain (Table S5). For the HEMI domain, we used the Emissions Database for Global Atmospheric Research (EDGARv4.2) (European Commission/Netherlands, 2016) for all anthropogenic emission sources (except aviation) with biogenic emissions from Global Emission Inventory Activity (Guenther et al., 1995). All these emissions are gridded, speciated, and temporalized as described in Xing et al. (2015) to generate model-ready emissions (Table S5). In both domains we used aircraft emissions generated from the Federal Aviation Administration's (FAA) Aviation Environmental Design Tool (AEDT) (Wilkerson et al., 2010). The U.S. EPA's National Emissions Inventory includes only Landing and Takeoff emissions, and until NEI-2011, they have used emissions estimates from the FAA's Emissions Dispersion Modeling System (EDMS). In addition, most CMAQ studies represented aircraft emissions only in the surface layer. Starting with Arunachalam et al. (2011), a new 4-D

Table 1
Modeling Configuration and Data Sources for HEMI and CONUS Domains

Category	HEMI 108 km	CONUS 36 km
Model version	CMAQv5.0.2	
Non-aviation emissions	EDGAR[a]-v4.2	NEI[a]-2005
Horizontal resolution	108 × 108 km^2	36 × 36 km^2
Vertical resolution	44 layers (top ~ 50 hPa)	
Meteorology	WRFv3.6 with MERRA[a] reanalysis data	
Aviation emissions	AEDT[a] (full flight)	
Boundary conditions	Clean air profile-based conditions (Byun & Ching, 1999; Mathur et al., 2017; Xing et al., 2015)	Downscaled from hemispheric CMAQ
Lightning NO_x emissions	Based on empirical calculation	Based on NLDN[a] observations

[a]NEI, National Emissions Inventory; EDGAR, Emissions Database for Global Atmospheric Research; MERRA, Modern-Era Retrospective Reanalysis; AEDT, Aviation Environmental Design Tool; NLDN, National Lightning Detection Network.

representation of aircraft emissions from EDMS was used in several studies including Woody et al. (2011), courtesy of a new tool that was developed called EDMS2Inv (Baek et al., 2012) to convert EDMS emissions for use in SMOKE and CMAQ. In recent years, several CMAQ applications (Vennam et al., 2014; Woody et al., 2015; Yim et al., 2015) have started using the new AEDT-based aircraft emissions. In this study we focused only on the commercial aircraft emissions and did not consider military emissions, which contribute 10–15% of total aircraft emissions (Olsen et al., 2013; Waitz et al., 2005). AEDT is an environment policy tool that estimates emissions for all global commercial flights throughout all phases of flight activity. These chorded emissions data (representing individual flight tracks modeled as series of chords or segments between all commercial airports) include fuel burn and key gaseous (CO, NO_x, SO_2, and VOC) and particulate matter (primary sulfate (PSO4), primary organic carbon (POC), and primary elemental carbon (PEC)) emissions for every individual flight (highly resolved both temporal and spatially). Note that AEDT has three primary $PM_{2.5}$ species directly emitted by aircraft, that is, PSO4, POC and PEC with emission estimates based on the first-order approximation version 3 (Wayson et al., 2009). We gridded these emissions using the AEDTProc (Baek et al., 2012) tool that allocates emissions both vertically and horizontally to the model grid. Lightning NO_x (LNO_x) emissions were calculated in the CONUS modeling domain based on the recent update available in CMAQ (Allen et al., 2012; Ott et al., 2010) that uses National Lightning Detection Network (NLDN) flash counts and the number of NO mol produced per unit flash. In the HEMI domain, due to the lack of flash count observational data outside the United States, we used the convective precipitation-based empirical approach for the entire domain. In this empirical approach, rather than constraining with observational data, constant values are used for number of flashes (147 flashes per hour per model column) and emissions (500 mol of NO) per flash (Allen et al., 2010, 2012; Pickering et al., 1998) throughout the modeling period. Note that using some of these constant values throughout the Northern Hemisphere can introduce some uncertainties in lightning emissions as these values can vary regionally.

Using these inputs, we carried out two annual simulations for both domains as shown in Table 2: (a) NoAirc: scenario with all sources of emissions except aviation and (b) Airc: scenario with all sources of emissions including aircraft emissions. We used boundary conditions from Airc108 (from Table 2) for both the NoAirc36 and Airc36 regional-scale simulations. We chose to use the same boundary conditions for both simulations because seasonal sensitivity simulations (for months of January and July) where we used different boundary conditions to drive the CONUS regional-scale simulations, once using Airc108 and once using NoAirc108, showed minimal differences in modeled impacts of aviation emissions in CONUS.

Table 2
Description of Modeling Scenarios

Model scenario	Domain	Description	Period
NoAirc36	CONUS	All source emissions (NEI) except aircraft	2005 with 1 month spin-up
Airc36	CONUS	All source emissions (NEI) including aircraft (AEDT)	2005 with 1 month spin-up
NoAirc108	HEMI	All source emissions (EDGAR) except aircraft	2005 with 3 month spin-up
Airc108	HEMI	All source emissions (EDGAR) including aircraft (AEDT)	2005 with 3 month spin-up

Most regional-scale annual modeling simulations for North America have used a 1–2 week spin-up period. We extended the spin-up period for the 36 km regional simulation to a full month to reduce initialization uncertainties. This approach is consistent with Hogrefe et al. (2017) who recommend that regional applications need more than 10 days spin-up. Whereas in hemispheric scale (108 km) some of the large-scale dynamics, transport processes (such as intercontinental) take >30 days; we thus decided to do a longer (3 months) spin-up for the hemispheric scale. The difference between Airc ($Conc_{Airc}$) and NoAirc ($Conc_{NoAirc}$) gives us the incremental concentrations that are attributable to the full-flight aircraft emissions, denoted as aviation-attributable contributions (AAC) in this study.

$$AAC = Conc_{Airc} - Conc_{NoAirc} \quad (1)$$

We also calculated the incremental contribution of aviation impacts when compared with all other source impacts defined as aviation contribution percentage (ACP) as follows:

$$ACP = \left(\frac{Conc_{Airc} - Conc_{NoAirc}}{Conc_{Airc}}\right) \times 100 \quad (2)$$

2.2. Observation Data

To evaluate our model predictions, we used surface observations from the Air Quality System network (AQS; http://www.epa.gov/aqs) for the United States in both the CONUS and HEMI domains. We also evaluated our model predictions in the upper troposphere using in situ aircraft observational data from the Intercontinental Chemical Transport Model (INTEX-NA) (Singh et al., 2006) and Measurement of OZone and water vapor by AIrbus in-service aircraft (MOZAIC; http://www.iagos.fr/web/rubrique3.html; Thouret et al., 2005) campaigns. Note that the INTEX-NA campaign was held in summer 2004, and it was one of the very few observation campaigns that measured middle and upper troposphere pollutant concentrations close to our model year 2005, so we considered this dataset for our model evaluation. The INTEX-NA campaign observations are confined only to the United States, but MOZAIC observational data include some major airports in other regions (Europe and Asia) of the HEMI domain. Note that Xing et al. (2015) evaluated the CMAQ-HEMI application in United States, Europe, and East Asia using surface monitoring data from those regions and found that the model was able to represent the observational patterns. We include the MOZAIC vertical evaluation in the supporting information (Figures S6 and S7).

2.3. Mass Flux

To better understand the vertical transport of aviation-attributable perturbations in the modeling domain, we computed and analyzed mass flux. Mass flux can be defined as the rate of the mass transferred across the model domain grid cell per unit time per unit area. To calculate mass flux of AAC, we followed the technique discussed in Klich and Fuelberg (2014). We considered vertical velocity (V_c) from meteorological (WRF) data and aviation-attributable concentrations for O_3 and $PM_{2.5}$ from model output. We converted model predicted mixing ratios (MR) to mass concentrations (M_c) and multiplied it by vertical velocity to obtain mass-based flux across each model layer as shown in equations (3) and (4). We named this metric as aviation-attributable mass flux (AMF). The positive vertical velocity indicates the updrafts occurring in the atmosphere, and the negative vertical velocity indicates the downdrafts occurring in the atmosphere. Therefore, a negative AMF indicates the downward transport of AAC mass and positive AMF indicates an upward transport of AAC mass.

$$M_c = MR \times 10^{-9} \times \left(\frac{MW_i}{MW_{air}}\right) \times DENS \quad (3)$$

where MR = model predicted mixing ratio (ppbv), MW_i = molecular weight of pollutant, MW_{air} = molecular weight of air, DENS = density of air (kg/m^3), and M_c = mass concentration (kg/m^3)

$$\text{Mass Flux} = M_c \times V_c \quad (4)$$

where V_c = vertical velocity from meteorology data (m/s) and mass flux (kg/m^2 s).

2.4. Isentropic Analysis

To illustrate the vertical transport of cruise altitude emissions to the surface and their seasonal variability, we conducted isentropic analysis. Pollutants (or air parcels) flowing along isentropes undergo both horizontal

Table 3
Domain-Wide Annual Average of Predicted O_3 (MDA8) and $PM_{2.5}$ Aviation-Attributable Contributions (AAC) for Overall HEMI Domain and the Subregions of the HEMI Domain: North America (HEMI-NA), Europe (HEMI-EU), and East Asia (HEMI-EA)

	O_3 (ppbv)		$PM_{2.5}$ ($\mu g/m^3$)	
Domain	Mean	Maximum	Mean	Maximum
HEMI	0.46 (1.3%)	1.92	0.013 (0.2%)	0.14
HEMI-NA	0.65 (1.7%)	1.03	0.021 (0.4%)	0.09
HEMI-EU	0.69 (1.9%)	0.94	0.031 (0.5%)	0.15
HEMI-EA	0.57 (1.5%)	1.05	0.021 (0.2%)	0.10

Note. The relative percentage of aircraft emission contribution when compared with all sources is shown in parentheses. Also shown are the maximum annual AAC in the domain for both pollutants.

and vertical transport. Therefore, we perform isentropic analysis, where we are correlating the isentropes with differences in concentrations to explain the vertical transport of cruise altitude emissions. The CMAQ model's vertically resolved concentrations and meteorological data are considered to conduct the isentropic analysis (Danielsen, 1961, 1968) for both hemispheric and regional domains. Note that we did not run the model using potential temperature θ as vertical coordinate system but postprocessed modeled aviation-attributable concentrations along the isentropic levels. We calculated potential temperature from meteorology data as follows for all model vertical layers.

$$\text{Theta}\ (T_h) = T \times \frac{P_s}{P_h}^{0.286} \quad (5)$$

where T is temperature at model vertical layers (K), P_s is surface pressure (Pa), and P_h is pressure at different model vertical layers (Pa).

We interpolated the model concentrations from vertical layers to calculated theta vertical levels (range 380–280 K).

3. Results and Discussion

3.1. Aviation Emissions Impact at Hemispheric Scale

3.1.1. Surface Analysis

We assessed the impacts of aviation emissions on surface air quality in the HEMI (108 km) domain, by calculating the model predicted aircraft-attributable contributions (AAC) as the difference between the simulations "with aviation" (Airc) and "without aviation" (NoAirc) as shown in equation (1). In other words, AAC are the aviation-attributable perturbations of pollutants due to aviation emissions. Model predicted hourly outputs were used to calculate various temporal (annual, monthly, and daily averages) and spatial (land grid cells domain average) metrics in this analysis. Throughout the study we used daily maximum 8 h average (MDA8) O_3 for surface analysis and hourly O_3 for vertical analysis. Table 3 shows the domain-wide annual average of the MDA8 O_3 and $PM_{2.5}$ AAC. As shown in Table 3 the model predicted AAC of 0.46 ppbv and 0.013 $\mu g/m^3$ for O_3 and $PM_{2.5}$, with maximum concentrations in the entire hemispheric domain reaching 1.92 ppbv and 0.14 $\mu g/m^3$. These results are consistent with the global-scale aviation surface impacts discussed in recent studies (Lee et al., 2013; Yim et al., 2015) that show annual perturbations of ~0.5–0.6 ppbv for O_3 and 0.006 $\mu g/m^3$ for $PM_{2.5}$ (see Table 4). Also shown in Tables 3 and 4 is the relative contribution of aviation when compared with impacts from all other sources as shown in equation (2). Overall, CMAQ-predicted values show that aviation impacts contribute 1.3% and 0.2% for O_3 and $PM_{2.5}$ at the surface in

Table 4
Summary Table Comparing the Aviation-Attributable Surface Impacts of O_3 and $PM_{2.5}$ From Other Studies With Our Study Results

Study	Model	Horizontal resolution latitude ×longitude (deg)	Average O_3 (ppbv)	Average $PM_{2.5}$ ($\mu g/m^3$)
Cameron et al. (2017)	GATOR-GCMOM (CRM)	4 × 5	0.046 (0.36%)	0.0772 (0.42%)
	GEOS-5 (CRM)	2 × 2.5	0.52 (1.92%)	−0.17 (−1.86%)
	NASA GISS Model2 (CTM)	2 × 2.5	0.17 (0.53%)	0.0062 (0.42%)
	NASA GISS Model2 (CRM)	2 × 2.5	0.32 (1.15%)	0.0165 (1.12%)
	CAM5 (CTM)	2 × 2.5	0.48 (1.80%)	0.0034 (0.21%)
	CAM5 (CRM)	2 × 2.5	0.37 (1.38%)	0.0133 (1.18%)
	GEOS-Chem (CTM)	4 × 5	0.43 (1.63%)	0.0007 (0.14%)
Yim et al. (2015)	Hybrid Model (GEOS-Chem, CMAQ, AERMOD)	4 × 5	0.6	0.006
Lee et al. (2013)	CAM-Chem (CTM)	2 × 2.5	> 1, 0.5 (July)	-
Jacobson et al. (2013)	GATOR-GCMOM (CRM)	4 × 5	0.05	0.54
This study	CMAQ (Northern Hemisphere Domain, CTM)	108 km (i.e., ~ 1 × 1)	0.46 (1.3%)	0.013 (0.2%)
This study	CMAQ (CONUS Domain, CTM)	36 km (regional scale)	0.03 (0.1%)	0.002 (0.1%)

Note. For each model we indicated in parentheses whether it is a chemistry transport model (CTM) or climate response model (CRM).

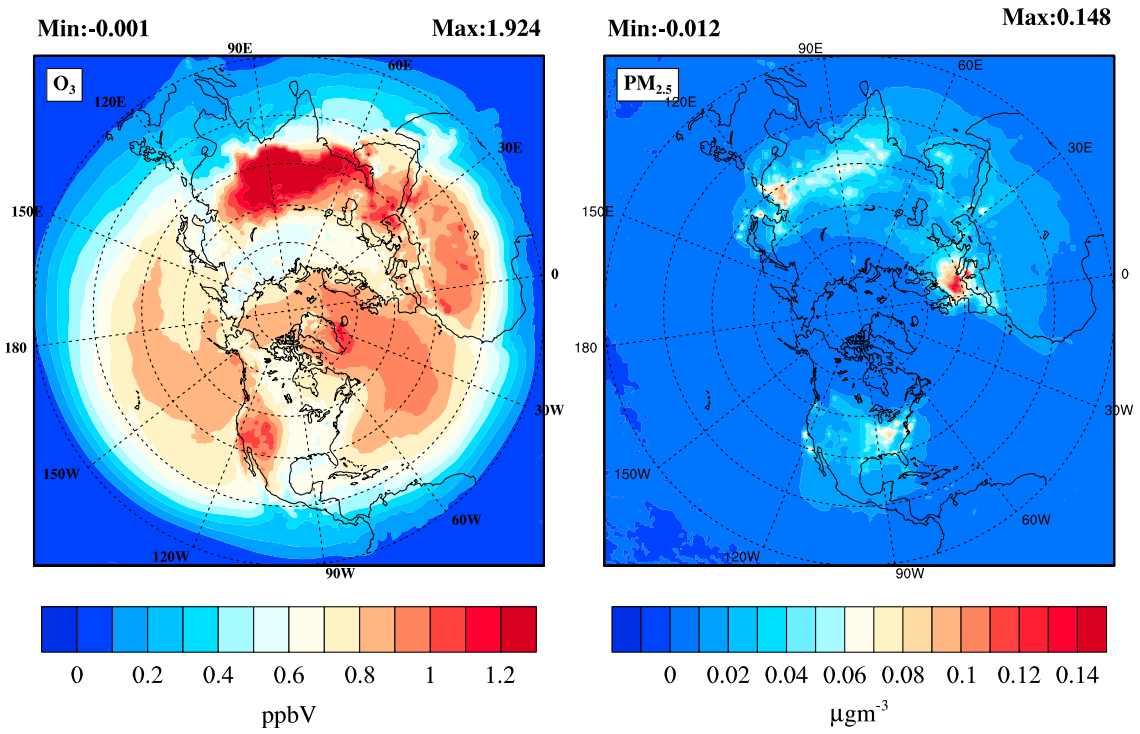

Figure 2. Aviation-attributable contributions of annual averaged (left) O_3 and (right) $PM_{2.5}$ for the hemispheric domain (HEMI) at the surface.

HEMI with slightly varying impacts in key subregions in Northern Hemisphere. EU shows the highest impacts of 1.9% (0.69 ppbv) and 0.5% (0.031 µg/m^3) for O_3 and $PM_{2.5}$. These values are ~1.4 times and ~2.2 times higher than the overall hemispheric average aviation impacts (O_3: 0.46 ppbv, $PM_{2.5}$: 0.013 µg/m^3). NA and EA show similar impacts as EU in the case of O_3, but the $PM_{2.5}$ impacts are lower when compared with EU.

Figure 2 shows the annual average AAC spatial plot for O_3 and $PM_{2.5}$ at the surface. In the HEMI domain, the maximum annual O_3 impacts occurred near Tibetan Plateau throughout the year. Monthly spatial plots (Figure S1) included in supporting information show similar spatial signal consistently in all months. This is comparable with other studies (Barrett et al., 2010), who reported that this impact was due to the relatively higher convective flux in the high-altitude region. Other than this hot spot, maximum annual impacts of ~0.8 ppbv are seen in the midlatitudes 30°N to 50°N band, with modest impacts near other high convective and warm weather regions such as the western United States and North Africa. In the case of $PM_{2.5}$, higher annual impacts occurred near major urban corridors such as the eastern United States, Western EU, and Eastern Asia (China) where aviation emissions and $PM_{2.5}$ precursor emissions are relatively high. This spatial signal is also shown in all months (Figure S2) with slightly higher maximum AAC during winter months.

We next focused on model predicted AAC for O_3 and $PM_{2.5}$ in three subregions with the highest aviation emissions. Figure 3 shows the spatial distribution of annual average AAC of O_3 and $PM_{2.5}$ in NA, EU, and EA. The maximum AAC for O_3 is comparable between the three subregions (NA: 1.03 ppbv, EU: 0.95 ppbv, and EA: 1.05 ppbv) with EA showing slightly higher impacts. In the NA subregion (Figure 3, top left), ~2 times higher impacts of O_3 occurs in western United States compared to eastern part of the country. In the EU subregion (Figure 3, middle row), higher impacts of ~0.8 ppbv of O_3 occur near Madrid, Munich, and Frankfurt. In EA subregion (Figure 3, bottom left), higher O_3 impacts are observed near the west side of EA (higher latitudes). Based on spatial distributions, the circulation and synoptic flow are important factors in the aviation-attributable O_3 perturbations.

The maximum $PM_{2.5}$ AAC of 0.145 µg/m^3 occurs in the EU subregion, which is ~1.42 and ~1.68 times higher when compared to the EA and NA regions. Among the total aviation-attributable $PM_{2.5}$ perturbations, we also saw that higher contribution came from inorganic aerosols (ammonium sulfate and ammonium nitrate),

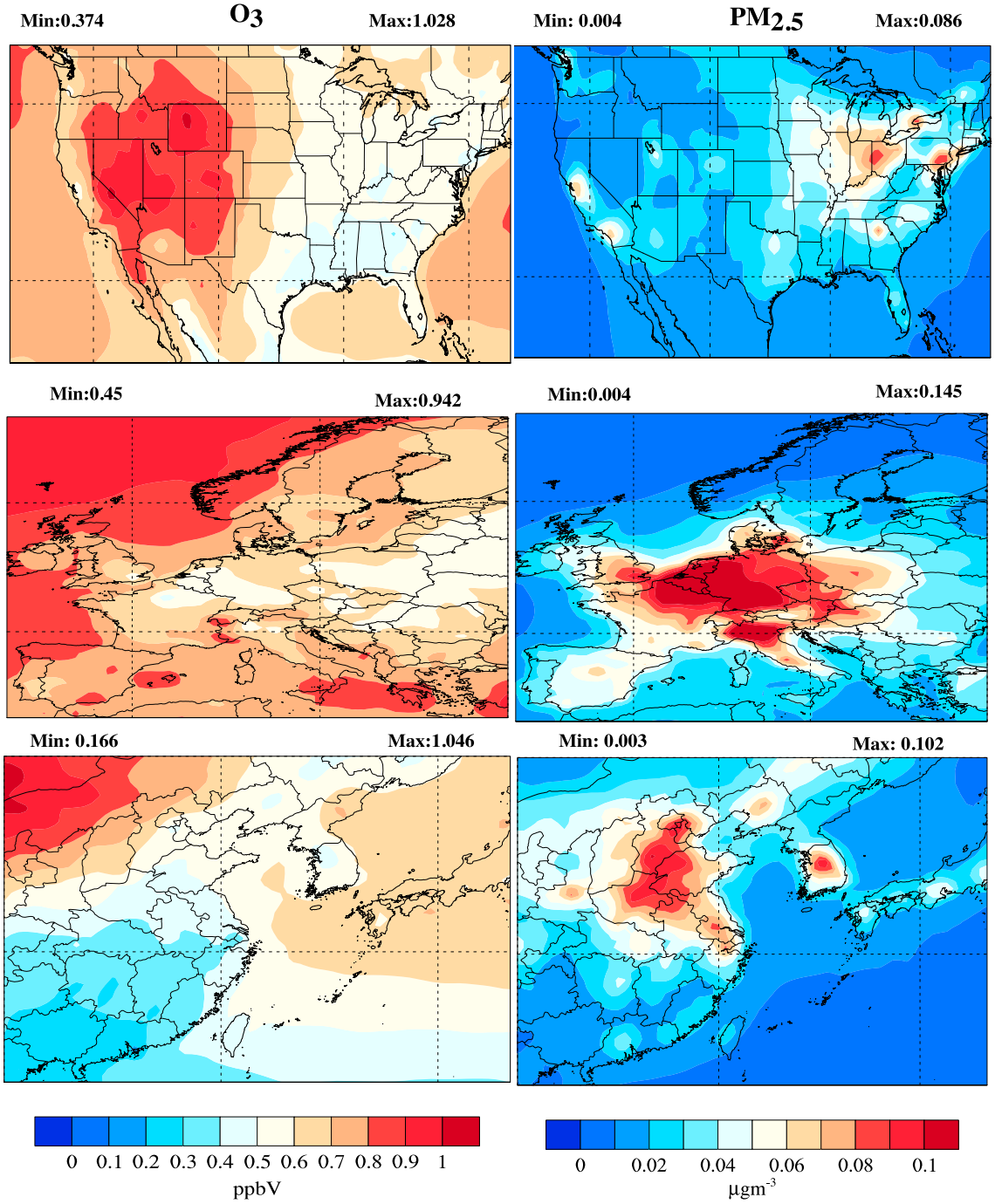

Figure 3. Aviation-attributable contributions of annual averaged (left column) O_3 and (right column) $PM_{2.5}$ at the surface for three subregions (top row) NA, (middle row) EU, and (bottom row) EA from hemispheric domain.

which are secondarily formed (not directly emitted from aircraft) in the atmosphere (details in Figure 4). This clearly indicates the influence of background emissions (such as ammonia emissions) in that region which increased the inorganic aerosol contribution. Similar finding that emphasized the role of background emissions has been clearly stated in previous studies (Arunachalam et al., 2011; Woody et al., 2011). In NA region, the annual average aviation-attributable $PM_{2.5}$ peaks of ~ 0.08 $\mu g/m^3$ are observed near urban regions and major airports such as LAX, ATL, JFK airports and the Ohio Valley region (Figure 3, top right). The increase of aviation-attributable $PM_{2.5}$ in Ohio Valley is mainly due to the ammonium nitrate aerosol,

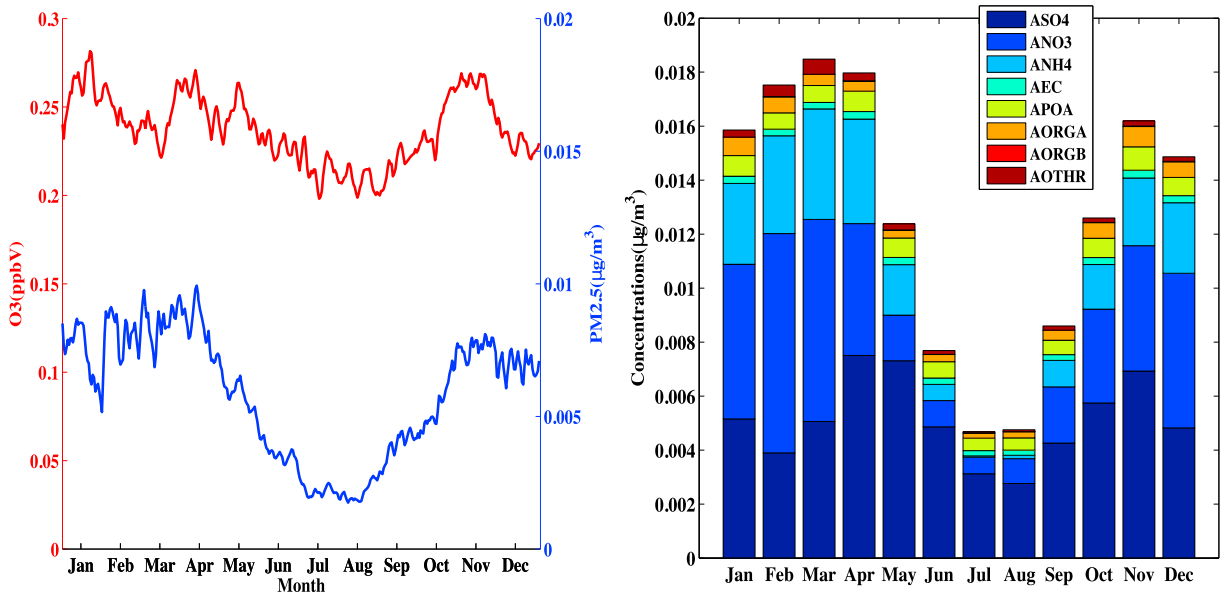

Figure 4. (left) Time series showing aviation-attributable domain-wide average of 8-hour daily maximum O_3 (red) and daily averaged $PM_{2.5}$ (blue) in the HEMI domain. (right) The domain wide average of monthly averaged speciated aerosol $PM_{2.5}$ AAC in the HEMI domain at the surface. *Speciated aerosols: ASO4 = sulfate, ANO3 = nitrate, ANH4 = ammonium, AEC = elemental carbon, APOA = primary organic, AORGA = anthropogenic secondary organic, AORGB = biogenic secondary organic, AOTHR = other aerosols.

where the aviation NO_x emissions reacted with free ammonia (Woody et al., 2011) in this region to increase aviation-attributable nitrate aerosol concentrations. In EU, higher $PM_{2.5}$ impacts of ~0.1–0.08 μg/m^3 are predicted in regions near Frankfurt, Munich, and London followed by regions near Madrid and Rome (~ 0.06 μg/m^3). In EA region, the highest impacts of ~0.1 μg/m^3 are observed near densely populated Beijing region followed by Shanghai and Seoul regions.

Figure 4 (left) shows the domain-wide average of MDA8 O_3 and daily averaged $PM_{2.5}$ AAC for HEMI domain throughout the entire year. As shown in Figure 4 (left), the winter months have up to ~ 1.5 times higher O_3 contributions than summer months with values in the range of ~0.2–0.3 ppbv. The higher winter impacts compared to summer are further explained in section 3.1.2. In the case of daily averaged $PM_{2.5}$, impacts in winter months are twice as seen in summer months. These seasonal $PM_{2.5}$ differences are mainly influenced by modeled inorganic aerosols (sulfate, nitrate, and ammonium) as shown in Figure 4 (right), which shows the monthly average individual speciated $PM_{2.5}$ predicted by the CMAQ model (sum of sulfate, nitrate, ammonium, elemental carbon, primary organic aerosol, secondary organic aerosol, and other crustal species). The speciated $PM_{2.5}$ shows that sulfate aerosol (ASO4) has larger contributions to total $PM_{2.5}$ during summer and fall months (April–November) than during winter months (December–March). During winter, nitrate aerosol (ANO3) is more prominent due to the presence of more HNO_3 (lesser reduction of HNO_3 through photolysis in winter season) to react with NH_3 to form nitrate aerosol and the semivolatile nature of nitrate leads to more of it in the particle phase at low temperatures. We also examined the seasonal cycle in the AAC for each subregion and speciated aerosols (Figure S3). In all three regions, the winter season impacts are slightly higher than summer impacts for both pollutants similar to the pattern observed in Figure 4.

3.1.2. Vertical Analysis

We studied the vertical profiles of O_3 and $PM_{2.5}$ impacts due to full-flight aviation emissions at different altitudes. Throughout this vertical analysis hourly O_3 and $PM_{2.5}$ concentrations at all model layers are used. The annual vertical impacts were averaged across three atmospheric regions: boundary layer (BL) of $<$2 km, mid-troposphere (MT) of 2–8 km, and upper troposphere (UT) of $>$8 km. Figure 5 (left) shows the annual average percentage contribution of AAC in the BL, MT, and UT regions for O_3. In the HEMI domain, the UT and MT impacts are ~2–2.3%, which is double the BL impacts. The subregions show ~1.2–2 times higher impacts than the overall HEMI impacts in all three vertical bins. In the case of O_3, EU shows higher impacts of ~4–4.5% in the MT and UT regions followed by EA and NA, which confirms that aviation impacts are higher in the upper

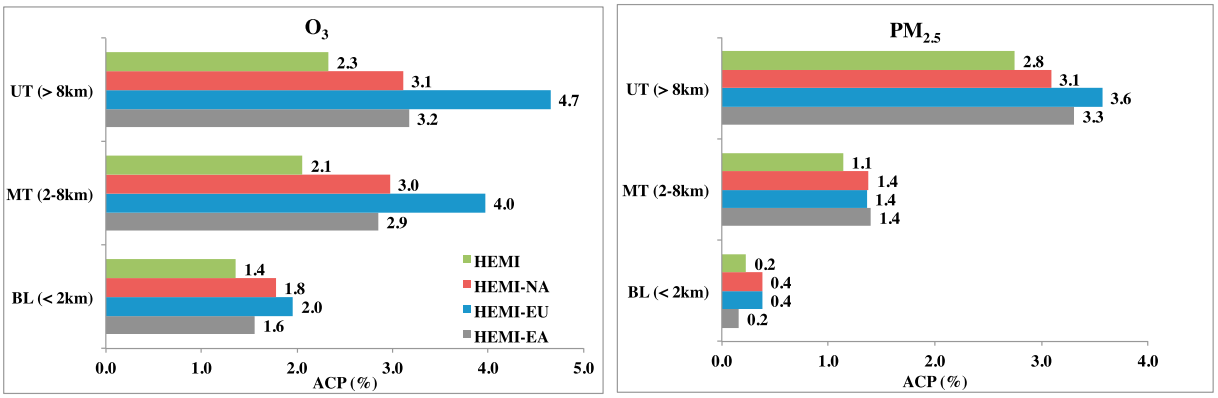

Figure 5. The aviation contribution percentage (ACP,%) to total annual average (left) O_3 and (right) $PM_{2.5}$ when compared with all other emission sources in the entire HEMI domain and for all three subregions of NA, EU, and EA. The vertical data are stratified into near boundary layer (BL), mid-troposphere (MT), and upper troposphere (UT).

altitudes than lower altitudes across all subregions. Figure 5 (right) shows the percentage contribution of AAC in BL, MT, and UT regions for $PM_{2.5}$. Overall across the HEMI domain, the UT impacts are estimated to be ~2.7%, which is ~2 times higher than MT impacts and 10 times higher than BL impacts. For $PM_{2.5}$ there are more decreases in predicted impacts near the BL region when compared with the UT region. The decreases in the BL region are larger for $PM_{2.5}$ than O_3.

To better quantify the vertical transport of the cruise altitude emissions, we calculated mass fluxes (using equations (3) and (4)) and performed an isentropic analysis. Figure 6 represents the aviation-attributable mass flux (AMF) vertical profile of O_3 and $PM_{2.5}$ in the HEMI domain; the general distribution (during all seasons) shows negative AMF (downward flux) near the UT region, with a change in direction toward positive AMF in the MT region (~3–4 km altitude) and changes to negative AMF near the surface. In the MT, the change in the direction is mainly due to the downward flux occurring in the upper altitudes and upward flux occurring in lower altitudes; therefore, the overall mass flux is influenced by both the upper altitude transport and surface mixing. Whereas in summer, as mixing is high near the surface the upward flux is predominant; hence, near the surface and in lower troposphere positive mass flux is seen in the vertical mass flux profiles.

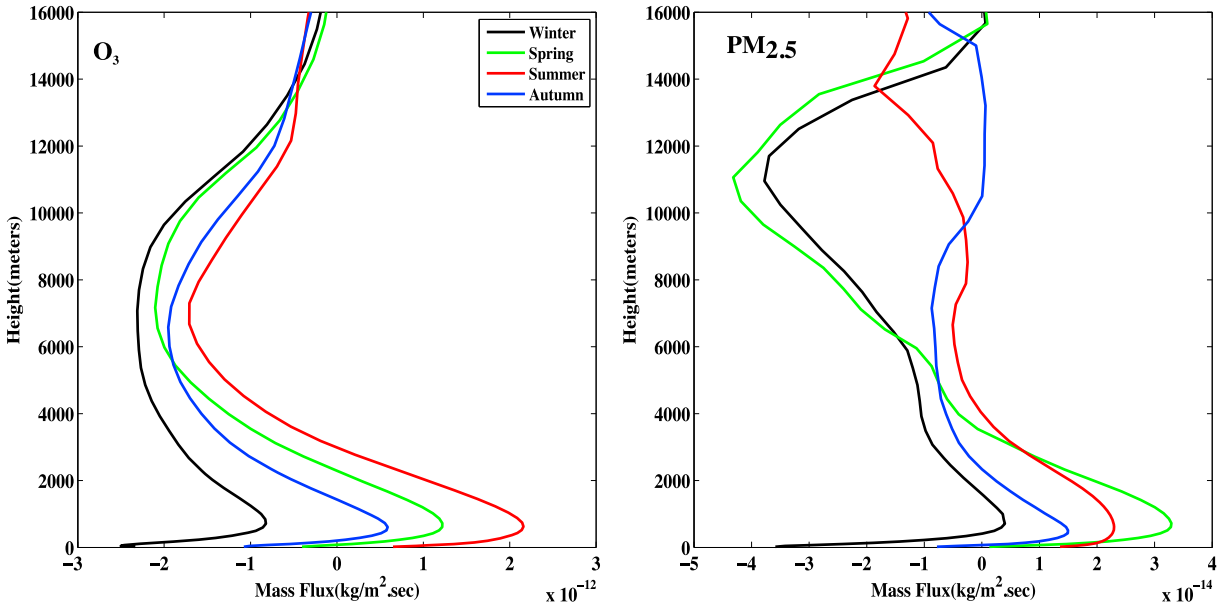

Figure 6. Vertical profiles of (left) O_3 and (right) $PM_{2.5}$ aviation-attributable mass flux (AMF) in the entire HEMI domain. Data averaged over each season in 2005 defined as winter: December–February, spring: March–May, summer: June–August, and Autumn: September–November.

The shape of the O_3 profile looks smooth and consistent in all seasons, with higher negative AMF during winter (December–February) and early spring (March). Even near the surface, winter months show more negative AMF due to lower photochemistry rates, higher downward transport, and more deep stratospheric intrusion events during winter and spring months. A recent CMAQ hemispheric study (Xing et al., 2016) saw similar higher impacts during winter months due to the downward transport from upper altitudes. This similar pattern of higher upper tropospheric ozone downward flux in winter and spring has been reported in another global model study (Yang et al., 2016).

In the case of $PM_{2.5}$, the vertical profiles vary seasonally highlighting the influence of seasonal factors such as humidity, temperature, clouds, precipitation, and deposition velocities on mass flux. For $PM_{2.5}$, winter and spring months show negative AMFs exceeding 3 kg m^{-2} s^{-1} (downdraft) near the UT region but not during summer and autumn months. Near the surface a similar downward flux (negative AMF) as seen in O_3 was predicted in winter months. This indicates that the transport of cruise altitude emissions emitted in the upper troposphere is highly influenced by the seasonal circulation pattern. Model predictions indicate downward transport only during winter months in the overall Northern Hemisphere when downdrafts/westerlies are high and boundary layer/surface mixing is low. As these transport phenomena and seasonal circulation change in different regions at hemispheric scales, we further analyzed mass flux profiles in individual subregions.

Figure 7, which shows AMF vertical profiles for both pollutants separated by regions and seasons, clearly indicates differences among the three subregions. In the case of O_3, near the UT region, a higher downward flux was predicted during the spring and autumn in NA, summer in EU, and winter in EA. Though the profiles show different profiles in the UT and MT, the near-surface profiles in the winter months consistently predicted a negative AMF for all three regions. A more negative AMF for O_3 is shown in EA during winter, indicating that the downward transport is higher due to a higher convection during winter monsoons in EA. The spatial and temporal changes in the vertical velocity mainly influence the AMF differences between various regions. Transport processes such as extratropical transport, monsoon circulation, and seasonal variation in tropopause height (which impact UTLS transport) are likely responsible for the seasonal differences in the AMF profiles particularly in UT and MT altitudes of various regions. Additional factors such as boundary mixing, oxidative capacity of different regions in various altitudes, and background concentrations can also influence the aviation-attributable perturbations. While we did not conduct further analysis of the meteorological data to explain the regional seasonal mass flux differences in detail, our goal is to emphasize the role of transport on regional aviation-attributable perturbations. The vertical velocity flux-based concentrations discussed here are based on the kinematic transport but do not clearly explain the reason behind the higher downward flux during winters. Since cruise altitude emissions occur mainly near the tropopause, a region where isentropic mixing/transport is important and highly influenced by potential temperature, we also studied the isentropic-based AAC for all seasons to understand the transport processes.

Isentropes are parallel potential temperature pathways, and ignoring diabatic effects represents the route that air parcels originating at cruise flight levels follow in the atmosphere. Figures 8 and 9 show the seasonal latitude-potential temperature cross-sectional plots (longitudinally averaged) to illustrate the transport of aviation-attributable concentrations of O_3 and $PM_{2.5}$ along isentropic levels. We vertically interpolated the concentrations along designated isentropic surfaces from 280 K to 380 K, by calculating potential temperature values for all model layers using equation (5). Figure 8 shows that across all seasons, a higher O_3 AAC occurs near 340–380 K isentropic surface (~ 9–16 km average altitude range). The midtroposphere (~320–300 K) isentropic surfaces get closer to the lower isentropes near higher latitudes (60–90 N) for all seasons. During winter season (Figure 8, top left), higher isentropes get closer to the lower isentropes close to the surface near midlatitudes (~ 40–60 N). Compared to other seasons, the O_3 AAC are higher during winter starting from below ~320 K, which indicates that the vertical downward transport of O_3 AAC along isentropes is enhanced. Similar results are reported in a recent study (Runde et al., 2016) that discussed the stratosphere-troposphere transport occurrence along 280–350 K isentropes in extratropics during the winter season. During summer season, the higher isentropic surfaces get closer to the near-surface isentropes farther north toward the pole. Additionally, in summer, higher isentropic surfaces show an upward pattern, which suggests that a portion of O_3 AAC follows isentropes into the lower stratosphere rather into the free troposphere.

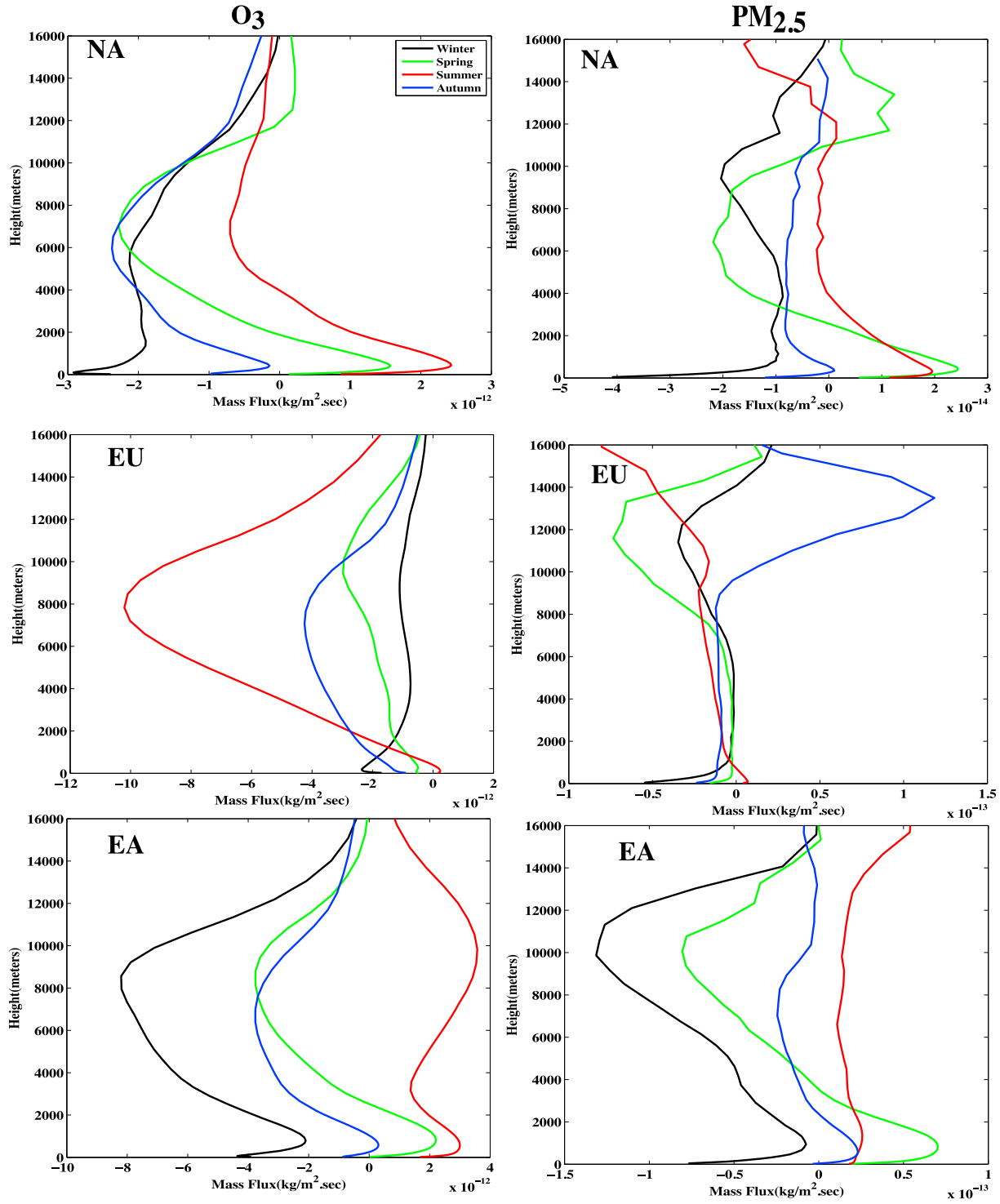

Figure 7. Vertical profiles of (left column) O_3 and (right column) $PM_{2.5}$ aviation-attributable mass flux (AMF) from (top row) NA, (middle row) EU, and (bottom row) EA subregions in the HEMI domain. The data are seasonally averaged similar to the description in Figure 6.

In the case of $PM_{2.5}$ AAC, as shown in Figure 9, the seasonal distributions vary significantly and thus emphasize the influence of precipitation patterns, wet deposition, chemical transformations, and cloud properties on PM intercontinental and vertical transport (Dentener et al., 2010). In Figure 9, during the winter and spring seasons the model predicted higher concentrations in upper isentropic levels around 360–340 K at

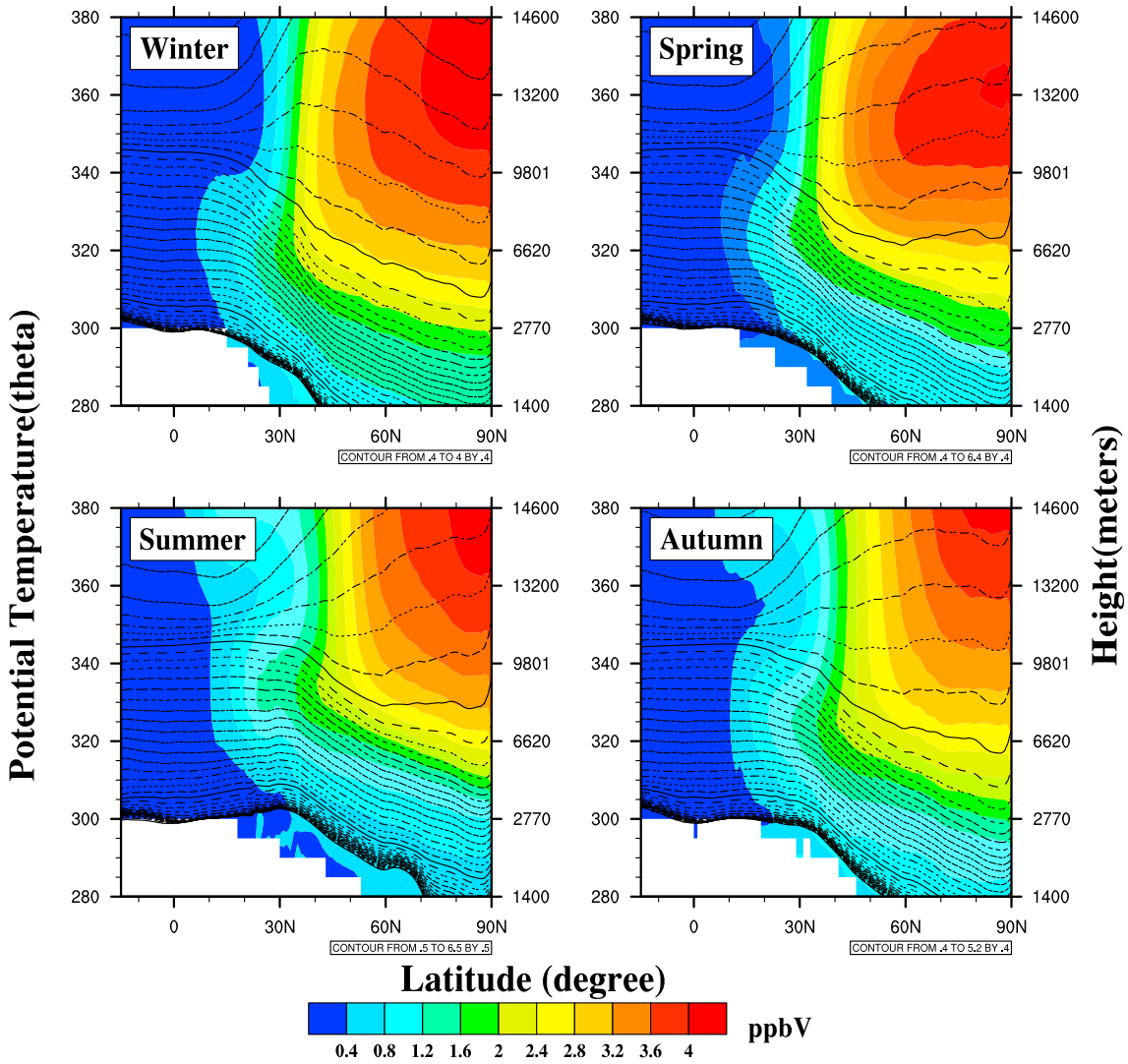

Figure 8. Latitude cross-sectional plot of seasonal average O_3 aviation-attributable concentrations interpolated along isentropic levels for all four seasons in the HEMI domain. The left axis represents the isentropic levels, right axis represents the average height for those isentropic model vertical levels, and bottom axis shows the latitudes in the HEMI domain. The black dashed overlay lines are the potential temperature (theta) in our modeling domain.

higher latitudes. Compared to the spring season, the winter season exhibits slightly higher AAC of $PM_{2.5}$ at lower isentropic levels between 320 and 280 K and transport of $PM_{2.5}$ AAC to the surface, similar to the pattern observed in O_3. The summer season shows relatively lower AAC both near the higher and lower isentropes. Another interesting feature of higher concentrations around 380 K isentrope near midlatitudes (25–50 N) was observed in summer, which indicates the upward transport of AAC during that season. The autumn season shows relatively higher $PM_{2.5}$ AAC in the MT region (340–300 K) than other seasons due to the higher nitrate aerosol and nitric acid (HNO_3) concentrations. The increase in NO_x concentrations during summer increased HNO_3 and nitrate aerosol concentrations during autumn seasons, which eventually increased $PM_{2.5}$ in MT region. The downward fluxes observed in vertical mass flux profiles and isentropic plots explain the transport of cruise altitude emissions during the winter season, and hence, higher impacts are observed at the surface in winter when compared to other seasons at the hemispheric scale. The main objective of isentropic analysis is to study the quasi-horizontal and vertical transport of aviation-attributable perturbations. While there are several other transport processes occurring in the atmosphere, illustrating those processes based on isentropic analysis is beyond the scope of this paper but can be an area of potential future research.

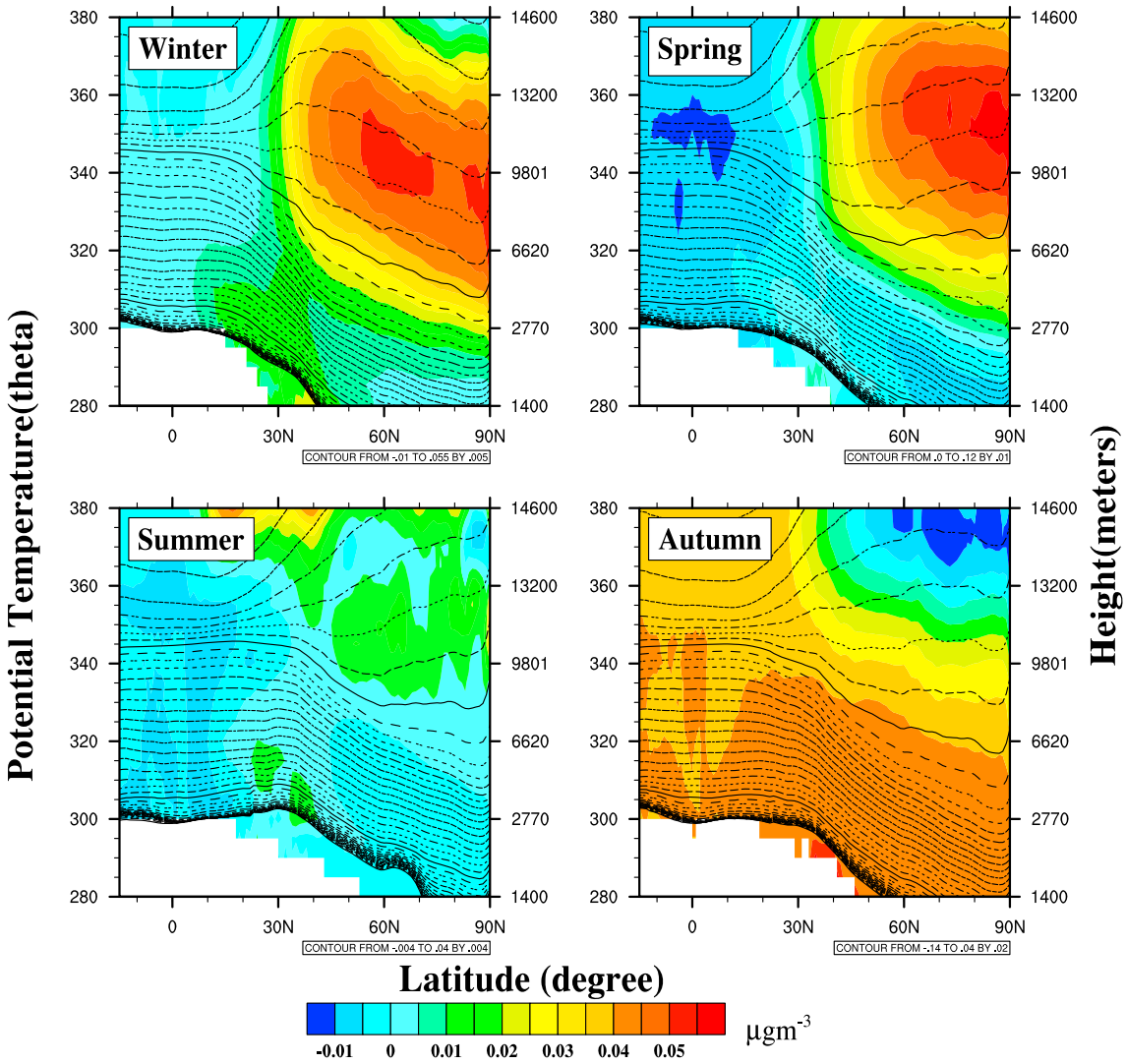

Figure 9. Latitude cross-sectional plot of seasonal average $PM_{2.5}$ aviation-attributable concentrations interpolated along isentropic levels for all four seasons in the HEMI domain. The left axis represents the isentropic levels, right axis represents the average height for those isentropic model vertical levels, and bottom axis shows the latitudes in the HEMI domain. The black dashed overlay lines are the potential temperature (theta) values in our modeling domain.

3.2. Grid Resolution Sensitivity

3.2.1. Model Evaluation

We evaluated the regional-scale 36 km (fine) CONUS and 108 km (coarse) NA model predictions with observations both near the surface and vertically. "Airc36" (all sources including aircraft, CONUS) and "Airc108" (all sources including aircraft, HEMI-NA) scenarios hourly model predictions are compared with AQS data near the surface for O_3 and $PM_{2.5}$. Note that along with grid resolution, the all-sources emission inventory is also different between these two scenarios, so any differences seen here are due to these two factors. For O_3, the annual Normalized Mean Bias (NMB, %) and Normalized Mean Error (NME, %) appear similar between both model scenarios; however, a few localized differences occur spatially (Figure S4). For example, the NMB from coarser resolution (Airc108) simulation for O_3 was −25% in the northeastern United States, while the NMB for the fine resolution (Airc36) simulation was only −10%. These low biases in coarse resolution simulation over the northeastern United States are likely due to the inability of the coarse resolution model to represent urban-scale emissions and processes. Temporal model performance was calculated by averaging seasonal NMB (%) during winter (December, January, February), spring (March, April, May), summer (June, July, August), and autumn (September, October, November).

Table 5
Seasonal Normalized Mean Bias (NMB, %) of Hourly O_3 and $PM_{2.5}$ Concentrations Predicted by Airc36 and Airc108 Model Scenarios in Comparison With Hourly AQS Observations

	O_3 (%)			$PM_{2.5}$ (%)		
Seasons	Airc36	Airc108	Difference	Airc36	Airc108	Difference
Winter	38.3	65.0	26.6	2.3	−24.9	−27.2
Spring	8.9	17.8	8.9	0.8	−14.7	−15.5
Summer	23.5	11.0	−12.4	−29.4	−58.5	−29.1
Autumn	34.2	41.7	7.5	−12.4	−44.0	−31.6

Note. All Airc108 predictions were limited to the NA region. Also shown are the normalized mean error (NMB, %) differences (Airc108 − Airc36) between scenarios. Winter: December–February, Spring: March–May, Summer: June–August, and Autumn: September–November.

Table 5 shows that the coarse resolution (NMB: ~11–65%) simulation showed higher overpredictions for O_3 compared to the fine resolution simulation (NMB: ~8–39%) during winter, spring, and autumn seasons. During summer, however, the fine resolution simulation showed ~12% higher overprediction than the coarse resolution simulation. In the case of $PM_{2.5}$, the model predicted an improvement in model performance for $PM_{2.5}$ at the finer horizontal resolution throughout all seasons (Table 5). Table S6 shows the NME seasonal differences. The coarse resolution showed consistently higher error than fine resolution for O_3 and $PM_{2.5}$ in all seasons. Overall, the annual average of NMB differences shows that the coarse resolution showed ~25% higher underpredictions in $PM_{2.5}$ and ~7% higher overpredictions in O_3 compared to the fine resolution.

Model predictions from three modeling scenarios Airc108 (all sources including aircraft), Airc36 (all sources including aircraft), and NoAirc36 (all sources without aircraft) for North America region are evaluated vertically with observations from the INTEX-NA campaign that occurred during 2004 as shown in Figure 10. Figure 10 shows vertical profiles of the model predicted concentrations of NO_2 and O_3 for July and August 2005 paired with INTEX observations from 2004. The paired data are binned based on the altitudes, and each point in the vertical profile represents the average of all the paired data that falls in that particular altitude bin. The number of pairs considered for calculating the average value in each bin differs (Figure 10, top and bottom right). Previous studies (Allen et al., 2012; Fang et al., 2010) showed that including lightning NO_x emissions reduced model error for O_3 and NO_x and pointed out the possibility of another missing emission source. In our study, the addition of lightning NO_x emissions and including aircraft full-flight emissions improved the model performance by decreasing the NME 5–11% for NO_2 (difference between Airc36 and NoAirc36) particularly in the upper troposphere (7–10 km). Figure 10 shows that the fine resolution simulation with aviation emissions (Airc36, red line) is closer to the observations than other model scenarios, although it should be noted that the NoAirc36 (green line) and Airc36 (red line) appear very close in Figure 10. However, by averaging all altitudes, NME values show an overall decrease of ~0.2%, ~4%, and ~2% (Table 6) for O_3, NO_2, and NO, respectively, in the model vertical column due to incorporating aircraft emissions aloft.

Overall, the model performance using the finer resolution simulation (Airc36) resulted in NME decreases of ~8%, ~16%, and ~9% for O_3, NO_2, and NO when compared with the coarse resolution simulation (Airc108) averaged over all altitudes. Also, note that in addition to the resolution the background emissions (anthropogenic, biogenic, and lightning emissions (Table 1)) used in Airc36 and Airc108 are also different, which could also influence some of the differences observed here. Model underprediction still exists in the case of NO, NO_2, and O_3 in 36 km, and this underprediction could be explained by the overprediction of the model for sink species such as PAN and HNO_3 (Figure S5). One explanation for this pattern was discussed in a prior study (Henderson et al., 2011), where the authors mentioned that photochemical models age NO_x too rapidly and chemical mechanisms convert it (partition ~25% total nitrogen) to HNO_3 in the UTLS region. We reiterate the prior study's findings that updating reaction rates as suggested in Henderson et al. (2011, 2012) in the chemical mechanism is important particularly to improve model performance near UTLS. Additionally, we also included model evaluation from the MOZAIC campaign near major airports in supporting information (Figures S6 and S7) to illustrate the model performance (in NMB %). We considered Beijing, Munich, New Delhi, and Shanghai airports (Figure S6) and observed that by incorporating the aircraft emissions the model performance improved (Figure S6, right). We also compared Airc108 and Airc36 O_3 concentrations at major airports in United States (Figure S7) and saw better performance with fine resolution.

3.2.2. Aviation Impacts Comparison

Figure 11 shows the spatial plot of annual average O_3 and $PM_{2.5}$ AAC at the surface in the 36 km CONUS domain. In the CONUS domain, the annual domain averages of AAC are 0.03 ppbv and 0.002 $\mu g/m^3$ for O_3 and $PM_{2.5}$, with maximum concentrations reaching 0.23 ppbv and 0.06 $\mu g/m^3$, respectively. Spatially, aviation impacts lower O_3 concentrations near major airports (in the grid cell containing the airport), primarily during winter months. Excess aviation NO_x reacts directly with O_3 (titration effect) and decreases AAC for O_3 near

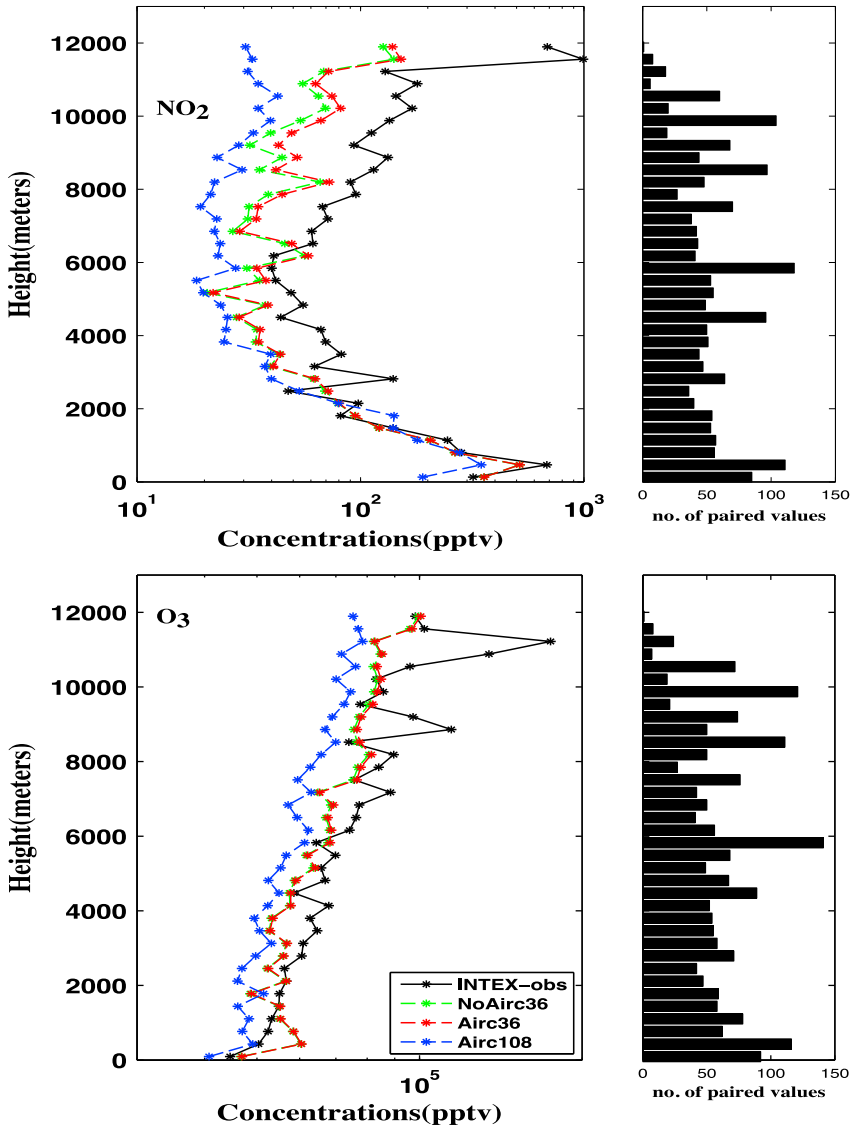

Figure 10. Comparison of modeled predictions of (top) NO_2 and (bottom) O_3 from scenarios NoAirc36 (green), Airc36 (red), and Airc108 (blue) paired with INTEX-NA observations (black) and binned vertically. Each point represents the mean concentration value in a particular altitude bin of paired modeled and observations. The bar plot (top and bottom right) shows the number of paired values in each bin.

Table 6
Normalized Mean Bias (%) Metric of O_3, NO_2, and NO From Three Model Scenarios NoAirc36, Airc36, Airc108 in Comparison With INTEX-NA Observations

	O_3			NO_2			NO		
Scenarios	Max	Min	Average	Max	Min	Average	Max	Min	Average
NoAirc36 (NMB, %)	19.8	−52.9	−8.41	46.5	−85.7	−38.1	−41.8	−84.1	−68.5
Airc36	20.1	−52.7	−7.75	50.9	−84.7	−34.3	−40.3	−83.3	−66.6
Airc108	−2.4	−55.1	−19.4	73.5	−96.6	−53.1	−34.5	−90.8	−76.5
Airc36-NoAirc36 (NME, %)	1.6	−1.3	−0.18	5.17	−11.7	−3.5	−0.1	−5.5	−1.9
Airc36-Airc108 (NME, %)	17.6	−21	−8.22	38.9	−56.9	−16.7	26.0	−32.6	−9.9

Note. Here we show the maximum, minimum, and average values of all altitudes (0–12 km). Also shown are the normalized mean error (%) differences between Airc36, NoAirc36, and Airc108 model scenarios.

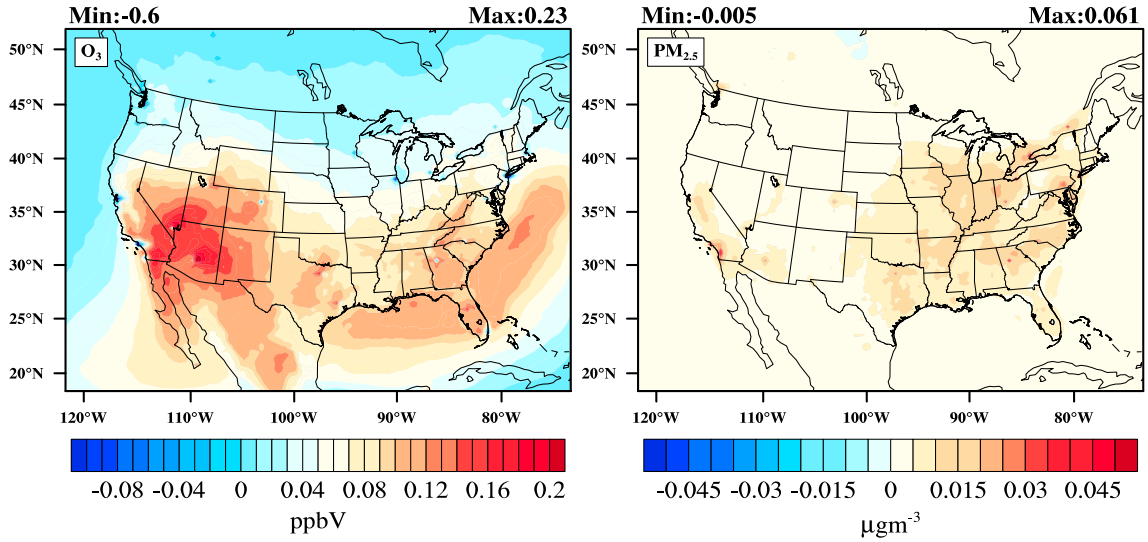

Figure 11. Annual average aviation-attributable contributions of (left) O_3 and (right) $PM_{2.5}$ for the CONUS (36 km) domain.

major airports. Increases of ~ 0.1–0.2 ppb were seen mainly near areas of high downward transport (western United States) and downwind of major airport areas: Atlanta (ATL), Houston (HOU), Dallas (DFW), and Phoenix (PHX). As shown in Figure 11 (right), $PM_{2.5}$ had higher impacts of ~ 0.04–0.06 μg/m^3 predicted near these major airport and urban areas: New York J.F. Kennedy (JFK), Chicago O'Hare (ORD), Atlanta Hartsfield (ATL), Los Angeles (LAX), eastern United States, Texas, and California.

When we compare the annual AAC of 36 km NA (CONUS, Figure 11) with 108 km NA (HEMI-NA, Figure 3 (top)) the overall spatial distribution looks similar (different contour levels); however, HEMI-NA shows considerably higher O_3 AAC in the western United States. The 36 km resolution simulation showed negative AAC near major airports and higher AAC downwind of these regions, differentiating the VOC- and NO_x-limited regions chemistry with excess aviation NO_x and titration effect, whereas the 108 km resolution did not capture these features. Due to these resolution differences, the seasonal variation in aviation impacts appeared to be different between the 36 km and 108 km NA regions. In the 36 km domain, summer months showed higher impacts than winter months (Figure S8), whereas in the 108 km NA domain we saw higher impacts during winter months.

In 36 km CONUS domain, CMAQ predicted annual domain-wide ACP of ~0.1% for both O_3 and $PM_{2.5}$, whereas in 108 km NA domain it was predicted to be 1.7% and 0.4%. The maximum annual AAC of O_3 in 108 km NA domain is predicted to be ~1 ppbv, which is ~5 times higher than the 36 km maximum AAC of O_3 (~0.2 ppbv). For $PM_{2.5}$, the maximum annual AAC predicted in 108 km NA domain is ~0.02 μg/m^3 higher than 36 km. In the vertical, the ACP for O_3 in 36 km and 108 km NA (Figure 5) domains near boundary layer, midtroposphere, and upper troposphere are ~0.16%, 0.4%, and 0.4% and ~1.8%, 2.4%, and 3.1%, respectively. For $PM_{2.5}$, these impacts are ~0.1%, 0.26%, and 0.48% and 0.4%, 1.4%, and 3% for 36 km and 108 km NA domains, respectively. Overall, the 108 km NA domain impacts of AAC are much higher when compared with the 36 km CONUS domain.

3.2.3. Emission Inventory Sensitivity

In all of the annual simulations discussed above, National Emissions Inventory (NEI) emissions were used for the CONUS domain and EDGAR emissions for the HEMI domain for nonaviation emissions (as shown in Table 1). Therefore, in our NA region coarse and fine-scale resolutions comparison, while an identical aircraft emission inventory was used, the nonaviation emission inventories are different. To address the inconsistencies and to make a consistent comparison that will facilitate potentially identical chemical regimes due to local sources within the CONUS domain, we ran two sensitivity simulations "Airc108_NEI" and "NoAirc108_NEI" by replacing the HEMI domain EDGAR with NEI emissions (consistent with CONUS domain) for NA region. These sensitivity simulations were conducted only for the months of January and July.

Table 7
Domain-Wide Monthly Average Aviation-Attributable Contributions (Rounded Up) (AAC) of O_3 and $PM_{2.5}$ From Model Scenarios (a) Airc108-NoAirc108 (HEMI-NA), (b) Airc108_NEI-NoAirc108_NEI (HEMI-NEI-NA), and (c) Airc36-NoAirc36 (CONUS)

	Month	HEMI-NA	HEMI-NEI-NA	CONUS	HEMI-NEI-NA/HEMI-NA	HEMI-NEI-NA/CONUS
O_3	Jan	0.69	0.70	0.01	1.0	70
	Jul	0.53	0.64	0.06	1.2	10
$PM_{2.5}$	Jan	0.027	0.027	0.002	1.0	13
	Jul	0.008	0.013	0.003	1.6	4

Note. Also shown are the ratio comparisons of these scenarios for January and July.

The Airc108 and Airc108_NEI model scenarios predictions were compared with AQS surface observations of O_3 (Figure S9) and $PM_{2.5}$ (Figure S10) for NA region. The 108 km with NEI emissions scenario (Airc108_NEI) improved model performance by reducing domain average NME by ~10% for both $PM_{2.5}$ and O_3 near urban areas. The overall NMB spatial pattern in HEMI-NEI-NA looks similar to the CONUS domain (Figures S9 and S10) with better model performance near urban regions due to better characterization of emissions from the bottom-up approach used in NEI. This change in model performance did impact the predicted AAC. Table 7 shows the domain-wide monthly AAC of O_3 and $PM_{2.5}$ from three modeling scenarios: (a) HEMI-NA, (b) HEMI-NEI-NA, and (c) CONUS. Table 7 also shows the fractional increase in AAC due to NEI emissions and finer grid resolution. Due to NEI emissions, the domain-wide average AAC increased ~1.2 and 1.6 times for O_3 and $PM_{2.5}$ during the summer month (July) in HEMI-NA region. However, larger differences in AAC occurred due to change in grid resolution. As shown in Table 7 the HEMI-NEI-NA scenario predicted ~70 (January) and ~10 (July) times higher AAC for O_3 and ~13 (January) and ~4 (July) times higher AAC for $PM_{2.5}$ when compared to CONUS domain. Note that these higher significant differences are only in the case of aviation-attributable perturbations. These differences occurred mainly near urban areas (Figures S11 and S12) where the fine resolution captured some of the decreases in concentrations due to aviation emissions, whereas the coarse resolution did not show this pattern. We also looked at the odd oxygen ($O_3 + NO_2 + 2NO_3 + 3N_2O_5$) metric (as shown in Figure S13) that is less sensitive to losses by titration. This metric also illustrates that the HEMI-NEI-NA (coarse) shows overall higher odd oxygen than compared to CONUS (fine). Overall, even the domain-wide daily average and maximum AAC were consistently higher in HEMI-NEI-NA case when compared to the CONUS case for both O_3 and $PM_{2.5}$ (Figures S14 and S15). We believe that the higher AAC in coarser resolution could be due to the relatively higher diffusion in upper model layers and high concentrations near airports with coarse horizontal grid. Tracer sensitivity simulations (for further details we refer to Vennam et al., 2013; Vennam, 2016) indicated that coarse resolution simulation transports upper altitudes perturbations more quickly (more diffusive with coarse grid) to lower altitudes than the fine resolution simulation as shown in Figures S16a and S16b. Due to the higher transport and overall higher aviation-attributable O_3 in the hemispheric domain, we also saw higher concentrations of aviation-attributable ozone over oceans (particularly in winter) due to deposition processes that contributed to the overall increase in domain-wide AAC. We believe that these are some of the reasons for higher AAC in the coarse resolution (HEMI, 108 km) simulation when compared to the fine (CONUS, 36 km) resolution simulation.

4. Conclusions

The key focus of this paper is to assess and quantify full-flight emissions impacts on air quality at hemispheric and regional modeling scales and to study the influence of horizontal grid resolution on aviation impacts. It is clear from our analyses that the grid resolution has the largest influence on model performance and AAC predictions when compared to just including full-flight emissions. Going from predictions relying on a coarse (108 km) resolution to those relying on a finer (36 km) resolution for North America improved the domain-wide average of NME by ~7% for O_3 and ~25% for $PM_{2.5}$. Vertically, the finer horizontal resolution model improved model performance by up to ~11% for NO_2 in the UTLS region. Averaged across all altitudes, the finer resolution model decreased NME by ~8%, ~16%, and ~9% for O_3, NO_2, and NO, respectively. Our results also highlight that by incorporating full-flight aircraft emissions at a fine resolution, the model performance was improved by up to ~ 5–11% for NO_2 in the UTLS region. For North America, AAC predictions using a 36 km resolution captured both titration effects during winter months and more rapid photochemistry during summer months. Predictions using the 108 km domain were incapable of capturing the local-scale

photochemistry effects and thus did not decrease O_3 AAC during winter when compared with summer. On the other hand, the CMAQ HEMI application captures the intercontinental long-range transport that can transport pollutants from higher altitudes to lower altitudes during periods of strong westerly winds, which increases the O_3 AAC during winter months.

At the hemispheric scale on an annual domain-average basis, aviation contributes only 1.3% and 0.2% for O_3 (0.69 ppbv) and $PM_{2.5}$ (0.03 $\mu g/m^3$) at the surface. Our results from CMAQ HEMI (for Northern Hemisphere) simulation are comparable to aviation-attributable surface impacts predicted by chemistry transport models in a recent study by Cameron et al. (2017). We also examined three subregions (EU, NA, and EA) that have significant aviation activity to emphasize the differences in impacts occurring at continental scales. This subregional analysis provides additional insights to support potential emissions reductions strategies, as the impacts can vary significantly by region. Among these three subregions, EU had the highest impacts, where aviation contributed ~1.9% and 0.5% for O_3 and $PM_{2.5}$ at the surface followed by NA and EA. The maximum O_3 impacts were predicted near midlatitudes 30°N to 50°N band, and maximum $PM_{2.5}$ aviation impacts were predicted near large airports throughout the Northern Hemisphere. The aviation contribution percentages (ACP) are ~ 2 times higher in the UT (2.3%) when compared with the surface (1.3%) for O_3, whereas for $PM_{2.5}$ the ACP is ~ 10 times higher in the UT (2.7%) than the surface (0.2%). Our analyses showed that the model-predicted AAC downward mass flux and vertical transport along the isentropes occurred particularly during winter months at hemispheric scales, indicating the influence of seasonal circulation patterns on vertical transport of cruise emissions in the model. Overall, the spatial distribution shows that the O_3 aviation impacts were driven by the atmospheric circulation and convective transport, while $PM_{2.5}$ aviation impacts were influenced by localized precursor emissions near urban regions.

The chemical processing and physical transport of aircraft emissions are heavily influenced by grid resolution. The use of a model that was 9 times more finely resolved horizontally made significant changes in the magnitude and location of AAC. The fine resolution (36 km) application at regional scale captured the nonlinearities in chemistry that are not captured by the coarser resolution; however, the use of a hemispheric scale (108 km) captures the intercontinental transport. Future studies should consider these changes in model implementations for studying aviation emissions. Therefore, running a nested fine-scale near-major aviation source regions (NA, EU, and EA) in a global/northern hemispheric model might capture both the fine-scale and global-scale intercontinental, transport, and chemistry processes in a more efficient manner. In addition, future modeling should also pay attention to the large-scale aviation forcing (boundary conditions) used to drive the regional-/fine-scale model. The comparison of grid resolution influence on aviation impacts needs to be reassessed in future analysis for longer periods (annual simulations) and by using consistent modeling platform (background emissions and boundary conditions) to address some of the limitations found in this study. Another limitation of this study is the absence of stratospheric chemistry in CMAQv5.0.2, which explains the model underpredictions near the UTLS region in our model evaluation. The presence of stratospheric chemistry in the UTLS region can also affect the NO_x and HO_x radical budgets that in turn influence the model predictions for O_3 and $PM_{2.5}$. Eastham et al. (2014) demonstrated the importance of stratospheric chemistry in upper altitudes (16–20 km) and showed how the unified stratospheric tropospheric chemistry reduced the overall global ozone column discrepancy from 9.9% to 3.6%. Therefore, not including detailed stratospheric chemistry in the model can influence the radical budget and oxidative capacity of troposphere, which can introduce uncertainties in the upper few model layers. Here in our study we do not have stratospheric chemistry for accurate representation of lower stratosphere; however, we do have the tropospheric chemistry occurring in the model upper layers, so it can still account for the fundamental ozone, NO_x photolysis reactions in the UTLS region. The lack of sufficient upper troposphere observation data is also one of the limitations in the study that restricted us from conducting model evaluation using observations from the same time period. Future studies should consider these changes in modeling implementations to further improve our understanding of aviation-attributable air quality impacts.

Acknowledgments
This work was funded by the Federal Aviation Administration through grants under the Partnership for AiR Transportation Noise & Emissions Reduction (PARTNER) (http://partner.mit.edu) and Aviation Sustainability Center (ASCENT) (http://ascent.aero) to the University of North Carolina at Chapel Hill. PARTNER and ASCENT are FAA/NASA/Transport Canada/US DOD/EPA-sponsored Centers of Excellence. The aircraft emissions inventories used for this work were provided by the U.S. Department of Transportation's Volpe Center. Any opinions, finding, and conclusions or recommendations expressed in this work are those of the author(s) and do not necessarily reflect the views of FAA or Volpe. We would like to acknowledge the European Commission for making the EDGAR inventory publicly available and Greet J. Maenhout from European Commission, Joint Research Centre (JRC) for providing us additional information and EDGAR data required for this study. The authors acknowledge the strong support of the European Commission, Airbus, and the Airlines (Lufthansa, Air-France, Austrian, Air Namibia, Cathay Pacific and China Airlines so far) who carry the MOZAIC or IAGOS equipment and perform the maintenance since 1994. MOZAIC is presently funded by INSU-CNRS (France), Météo-France, CNES, Université Paul Sabatier (Toulouse, France), and Research Center Jülich (FZJ, Jülich, Germany). IAGOS has been and is additionally funded by the EU projects IAGOS-DS and IAGOS-ERI. The MOZAIC-IAGOS data are available via CNES/CNRS-INSU Ether Web site http://www.pole-ether.fr. We would also like to acknowledge Barron Henderson from the U.S. Environmental Protection Agency (EPA) for providing INTEX campaign observations, Bok Haeng Baek from the UNC Institute for the Environment for developing the AEDTProc tool, and Matthew C. Woody from the U.S. EPA for technical discussions. Although this work has been reviewed and approved for publication by the U.S. EPA, it does not necessarily reflect the views and policies of the agency. We acknowledge the three anonymous peer reviewers whose comments and suggestions greatly enhanced this manuscript. The readers are requested to contact the corresponding author for the data that support the analysis and conclusions of this work.

References

Allen, D., Pickering, K., Duncan, B., & Damon, M. (2010). Impact of lightning NO emissions on North American photochemistry as determined using the Global Modeling Initiative (GMI) model. *Journal of Geophysical Research*, *115*, D22301. https://doi.org/10.1029/2010JD014062

Allen, D. J., Pickering, K. E., Pinder, R. W., Henderson, B. H., Appel, K. W., & Prados, A. (2012). Impact of lightning-NO on eastern United States photochemistry during the summer of 2006 as determined using the CMAQ model. *Atmospheric Chemistry and Physics*, *12*, 1737–1758. https://doi.org/10.5194/acp-12-1737-2012

Anenberg, S. C., West, I. J., Fiore, A. M., Jaffe, D. A., Prather, M. J., Bergmann, D., … Zeng, G. (2009). Intercontinental impacts of ozone pollution on human mortality. *Environmental Science & Technology*, *43*, 6482–6487. https://doi.org/10.1021/es900518z

Appel, K. W., Foley, K. M., Bash, J. O., Pinder, R. W., Dennis, R. L., Allen, D. J., & Pickering, K. (2011). A multi-resolution assessment of the Community Multiscale Air Quality (CMAQ) model v4. 7 wet deposition estimates for 2002–2006. *Geoscientific Model Development*, *4*, 357–371. https://doi.org/10.5194/gmd-4-357-2011

Appel, K. W., Napelenok, S. L., Foley, K. M., Pye, H. O., Hogrefe, C., Luecken, D. J., … Hutzell, W. T. (2017). Description and evaluation of the Community Multiscale Air Quality (CMAQ) modeling system version 5.1. *Geoscientific Model Development*, *10*(4), 1703–1732. https://doi.org/10.5194/gmd-10-1703-2017

Arunachalam, S., Wang, B., Davis, N., Baek, B. H., & Levy, J. I., (2011). Effect of chemistry- transport model scale and resolution on population exposure to $PM_{2.5}$ from aircraft emissions during landing and takeoff. *Atmospheric Environment*, *45*(19), 3294–3300.

Baek, B. H., Arunachalam, S., Woody, M., Vennam, L. P., Omary, M., Binkowski, F., & Fleming, G. (2012). A new interface to model global commercial aircraft emissions from the FAA Aviation Environmental Design Tool (AEDT) in air quality models. Chapel Hill, NC: Annual CMAS Conference, 15–17 October, 2012.

Barrett, S. R. H., Britter, R. E., & Waitz, I. A. (2010). Global mortality attributable to aircraft cruise emissions. *Environmental Science and Technology*, *44*, 7736–7742. https://doi.org/10.1021/es101325r

Baughcum, S. L., Sutkus Jr., D. J., & Hendersonm, S. C. (1998). Year 2015 Aircraft Emission Scenario for Scheduled Air Traffic, NASA-CR-1998-207638.

Beck, J. P., Reeves, C. E., de Leeuw, F. A. A. M., & Penkett, S. A. (1992). The effect of aircraft emissions on tropospheric ozone in the Northern Hemisphere. *Atmospheric Environment. Part A. General Topics*, *26*(1), 17–29. https://doi.org/10.1016/0960-1686(92)90257-L

Byun, D. W., & Ching, J. K. S. (Eds.) (1999). *Science Algorithms of the EPA Models-3 Community Multiscale Air Quality (CMAQ) Modeling System*. Washington, DC: US Environmental Protection Agency, Office of Research and Development.

Byun, D. W., & Schere, K. (2006). Review of the governing equations, computational algorithms, and other components of the models-3 Community Multiscale Air Quality (CMAQ) modeling system. *Applied Mechanics Reviews*, *59*, 51–57. https://doi.org/10.1115/1.2128636

Cameron, M. A., Jacobson, M. Z., Barrett, S. R. H., Bian, H., Chen, C. C., Eastham, S. D., … Unger, N. (2017). An intercomparative study of the effects of aircraft emissions on surface air quality. *Journal of Geophysical Research: Atmospheres*, *122*, 8325–8344. https://doi.org/10.1002/2016JD025594

Danielsen, E. F. (1961). Trajectories: Isobaric, isentropic and actual. *Journal of Meteorology*, *18*(4), 479–486. https://doi.org/10.1175/1520-0469(1961)018%3C0479:TIIAA%3E2.0.CO;2

Danielsen, E. F. (1968). Stratospheric-tropospheric exchange based on radioactivity, ozone and potential vorticity. *Journal of the Atmospheric Sciences*, *25*(3), 502–518. https://doi.org/10.1175/1520-0469(1968)025%3C0502:STEBOR%3E2.0.CO;2

Dentener, F., Keating, T., & Akimoto, H. (2010). *Hemispheric Transport of 2010 Part A: Ozone and Particulate Matter*, *Air Pollut. Stud* (Vol. 17). New York: United Nations Publications.

Eastham, S. D., Weisenstein, D. K., & Barrett, S. R. H. (2014). Development and evaluation of the unified tropospheric–stratospheric chemistry extension (UCX) for the global chemistry-transport model GEOS-Chem. *Atmospheric Environment*, *89*, 52–63. https://doi.org/10.1016/j.atmosenv.2014.02.001

European Commission, J. R. C. (JRC)/Netherlands E. A. A. (PBL) (2016). Emission database for global atmospheric research (EDGAR). [Retrieved from http://edgar.jrc.ec.europa.eu.]. (March 1, 2016)

Fang, Y., Fiore, A. M., Horowitz, L. W., Levy, H., Hu, Y., & Russell, A. G. (2010). Sensitivity of the NO_y budget over the United States to anthropogenic and lightning NO_x in summer. *Journal of Geophysical Research*, *115*, D18312. https://doi.org/10.1029/2010JD014079

Finlayson-Pitts, B. J., & Pitts, J. N. Jr. (2000). Chapter 2—The atmospheric system. In *Chemistry of the Upper and Lower Atmosphere* (pp. 15–42). San Diego, CA: Academic Press. https://doi.org/10.1016/B978-012257060-5/50004-6

Gardner, R. M., Adams, K., Cook, T., Deidewig, F., Ernedal, S., Falk, R., … van Drimmelen, R. (1997). The ANCAT/EC global inventory of NO_x emissions from aircraft. *Atmospheric Environment*, *31*(12), 1751–1766. https://doi.org/10.1016/S1352-2310(96)00328-7

Gauss, M., Isaksen, I. S. A., Lee, D. S., & Søvde, O. A. (2006). Impact of aircraft NO_x emissions on the atmosphere—Tradeoffs to reduce the impact. *Atmospheric Chemistry and Physics*, *6*, 1529–1548. https://doi.org/10.5194/acp-6-1529-2006

Guenther, A., Hewitt, C. N., Erickson, D., Fall, R., Geron, C., Graedel, T., … Zimmerman, P. (1995). A global model of natural volatile organic compound emissions. *Journal of Geophysical Research*, *100*(D5), 8873–8892. https://doi.org/10.1029/94JD02950

Henderson, B. H., Akhtar, F., Pye, H. O. T., Napelenok, S. L., & Hutzell, W. T. (2014). A database and tool for boundary conditions for regional air quality modeling: Description and evaluation. *Geoscientific Model Development*, *7*(1), 339–360. https://doi.org/10.5194/gmd-7-339-2014

Henderson, B. H., Pinder, R. W., Crooks, J., Cohen, R. C., Carlton, A. G., Pye, H. O. T., & Vizuete, W. (2012). Combining Bayesian methods and aircraft observations to constrain the HO.+ NO 2 reaction rate. *Atmospheric Chemistry and Physics*, *12*, 653–667. https://doi.org/10.5194/acp-12-653-2012

Henderson, B. H., Pinder, R. W., Crooks, J., Cohen, R. C., Hutzell, W. T., Sarwar, G., … Vizuete, W. (2011). Evaluation of simulated photochemical partitioning of oxidized nitrogen in the upper troposphere. *Atmospheric Chemistry and Physics*, *11*, 275–291. https://doi.org/10.5194/acp-11-275-2011

Hogrefe, C., Roselle, S. J., & Bash, J. O. (2017). Persistence of initial conditions in continental scale air quality simulations. *Atmospheric Environment*, *160*, 36–45. https://doi.org/10.1016/j.atmosenv.2017.04.009

Holloway, T., Fiore, A., & Hastings, M. G. (2003). Intercontinental transport of air pollution: Will emerging science lead to a new hemispheric treaty? *Environmental Science and Technology*, *37*(20), 4535–4542. https://doi.org/10.1021/es034031g

Houyoux, M. R., Vukovich, J. M., Coats, J. C. Jr., Wheeler, N. J. M., & Kasibhatla, P. S. (2000). Emission inventory development and processing for the seasonal model for regional air quality (SMRAQ) project. *Journal of Geophysical Research*, *105*(D7), 9079–9090. https://doi.org/10.1029/1999JD900975

Jacob, D. J., Logan, J. A., & Murti, P. P. (1999). Effect of rising Asian emissions on surface ozone in the United States. *Geophysical Research Letters*, *26*(14), 2175–2178. https://doi.org/10.1029/1999GL900450

Jacobson, M. Z., Wilkerson, J. T., Naiman, A. D., & Lele, S. K. (2011). The effects of aircraft on climate and pollution. Part I: Numerical methods for treating the subgrid evolution of discrete size- and composition-resolved contrails from all commercial flights worldwide. *Journal of Computational Physics*, *230*, 5115–5132. https://doi.org/10.1016/j.jcp.2011.03.031

Jacobson, M. Z., Wilkerson, J. T., Naiman, A. D., & Lele, S. K. (2013). The effects of aircraft on climate and pollution. Part II: 20-year impacts of exhaust from all commercial aircraft worldwide treated individually at the subgrid scale. *Faraday Discussions*, *165*, 369–382. https://doi.org/10.1039/c3fd00034f

Jaegle, L. (2007). Pumping up surface air. *Science*, *315*, 772–773. https://doi.org/10.1126/science.1138988

Jaffe, D., Anderson, T., Covert, D., Kotchenruther, R., Trost, B., Danielson, J., … Uno, I. (1999). Transport of Asian air pollution to North America. *Geophysical Research Letters*, *26*(6), 711–714. https://doi.org/10.1029/1999GL900100

Kentarchos, A. S., & Roelofs, G. J. (2002). Impact of aircraft NO_x emissions on tropospheric ozone calculated with a chemistry-general circulation model: Sensitivity to higher hydrocarbon chemistry. *Journal of Geophysical Research*, *107*(D13), 4175. https://doi.org/10.1029/2001JD000828

Klich, C. A., & Fuelberg, H. E. (2014). The role of horizontal model resolution in assessing the transport of CO in a middle latitude cyclone using WRF-Chem. *Atmospheric Chemistry and Physics*, *14*(2), 609–627. https://doi.org/10.5194/acp-14-609-2014

Kohler, M. O., Radel, G., Dessens, O., Shine, K. P., Rogers, H. L., Wild, O., & Pyle, J. A. (2008). Impact of perturbations to nitrogen oxide emissions from global aviation. *Journal of Geophysical Research*, *113*, D11305. https://doi.org/10.1029/2007JD009140

Lam, Y. F., & Fu, J. S. (2009). A novel downscaling technique for the linkage of global and regional air quality modeling. *Atmospheric Chemistry and Physics*, *9*, 9169–9185. https://doi.org/10.5194/acp-9-9169-2009

Lamarque, J.-F., Emmons, L. K., Hess, P. G., Kinnison, D. E., Tilmes, S., Vitt, F., … Tyndall, G. K. (2012). CAM-chem: Description and evaluation of interactive atmospheric chemistry in the Community Earth System Model. *Geoscientific Model Development*, *5*, 369–411. https://doi.org/10.5194/gmd-5-369-2012

Lee, H., Olsen, S. C., Wuebbles, D. J., & Youn, D. (2013). Impacts of aircraft emissions on the air quality near the ground. *Atmospheric Chemistry and Physics*, *13*(11), 5505–5522. https://doi.org/10.5194/acp-13-5505-2013

Leibensperger, E. M., Mickley, L. J., Jacob, D. J., & Barrett, S. R. H. (2011). Intercontinental influence of NO_x and CO emissions on particulate matter air quality. *Atmospheric Environment*, *45*, 3318–3324. https://doi.org/10.1016/j.atmosenv.2011.02.023

Lin, C., Jacob, D. J., Munger, J. W., & Fiore, A. M. (2000). Increasing background ozone in surface air over the United States. *Geophysical Research Letters*, *27*, 3465–3468.

Lin, J., Pan, D., Davis, S. J., Zhang, Q., He, K., Wang, C., … Guan, D. (2014). Chinas international trade and air pollution in U.S. *Proceedings of the National Academy of Sciences of the United States of America*, *111*(5), 1736–1741. https://doi.org/10.1073/pnas.1312860111

Ma, P. L., Rasch, P. J., Fast, J. D., Easter, R. C., Gustafson, W. I., Liu, X., … Singh, B. (2014). Assessing the CAM5 physics suite in the WRF-Chem model: Implementation, resolution sensitivity, and a first evaluation for a regional case study. *Geoscientific Model Development*, *7*(3), 755–778. https://doi.org/10.5194/gmd-7-755-2014

Ma, P. L., Rasch, P. J., Wang, M., Wang, H., Ghan, S. J., Easter, R. C., … Ma, H.-Y. (2015). How does increasing horizontal resolution in a global climate model improve the simulation of aerosol-cloud interactions? *Geophysical Research Letters*, *42*, 5058–5065. https://doi.org/10.1002/2015GL064183

Mathur, R., Gilliam, R., Bullock, O. R. Jr., Roselle, S., Pleim, J., Wong, D., … Streets, D. (2012). Extending the applicability of the community multiscale air quality model to hemispheric scales: Motivation, challenges, and progress. In *Air Pollution Modeling and its Application XXI* (pp. 175–179).

Mathur, R., Xing, J., Gilliam, R., Sarwar, G., Hogrefe, C., Pleim, J., … Young, J. (2017). Extending the Community Multiscale Air Quality (CMAQ) modeling system to hemispheric scales: Overview of process considerations and initial applications. *Atmospheric Chemistry and Physics*, *17*(20), 12,449–12,474. https://doi.org/10.5194/acp-17-12449-2017

Olsen, S. C., Wuebbles, D. J., & Owen, B. (2013). Comparison of global 3-D aviation emissions datasets. *Atmospheric Chemistry and Physics*, *13*(1), 429–441. https://doi.org/10.5194/acp-13-429-2013

Ott, L. E., Pickering, K. E., Stenchikov, G. L., Allen, D. J., DeCaria, A. J., Ridley, B., … Tao, W. K. (2010). Production of lightning NO_x and its vertical distribution calculated from three-dimensional cloud-scale chemical transport model simulations. *Journal of Geophysical Research*, *115*, D04301. https://doi.org/10.1029/2009JD011880

Penner, J. E., Lister, D. H., Griggs, D. J., Dokken, D. J., & McFarland, M. (1999). *Aviation and the Global Atmosphere—A Special Report of IPCC Working Groups I and III*. Intergovernmental Panel on Climate Change (365 pp.). Cambridge, UK and New York: Cambridge University Press.

Pickering, K. E., Wang, Y., Tao, W.-K., Price, C., & Müller, J.-F. (1998). Vertical distributions of lightning NO_x for use in regional and global chemical transport models. *Journal of Geophysical Research*, *103*(D23), 31,203–31,216. https://doi.org/10.1029/98JD02651

Reidmiller, D. R., Fiore, A. M., Jaffe, D. A., Bergmann, D., Cuvelier, C., Dentener, F. J., … Zuber, A. (2009). The influence of foreign vs. North American emissions on surface ozone in the US. *Atmospheric Chemistry and Physics*, *9*, 5027–5042. https://doi.org/10.5194/acp-9-5027-2009

Rienecker, M. M., Suarez, M. J., Gelaro, R., Todling, R., Bacmeister, J., Liu, E., … Woollen, J. (2011). MERRA: NASA's modern-era retrospective analysis for research and applications. *Journal of Climate*, *24*, 3624–3648. https://doi.org/10.1175/JCLI-D-11-00015.1

Runde, T., Dameris, M., Garny, H., & Kinnison, D. (2016). Classification of stratospheric extreme events according to their downward propagation to the troposphere. *Geophysical Research Letters*, *43*(12), 6665–6672. https://doi.org/10.1002/2016GL069569

Sarwar, G., Appel, K. W., Carlton, A. G., Mathur, R., Schere, K., Zhang, R., & Majeed, M. A. (2011). Impact of a new condensed toluene mechanism on air quality model predictions in the U.S. *Geoscientific Model Development*, *4*, 183–193. https://doi.org/10.5194/gmd-4-183-2011

Sarwar, G., Simon, H., Xing, J., & Mathur, R. (2014). Importance of tropospheric ClNO2 chemistry across the Northern Hemisphere. *Geophysical Research Letters*, *41*(11), 4050–4058. https://doi.org/10.1002/2014GL059962

Singh, H. B., Brune, W. H., Crawford, J. H., Jacob, D. J., & Russell, P. B. (2006). Overview of the summer 2004 Intercontinental Chemical Transport Experiment-North America (INTEX-A). *Journal of Geophysical Research*, *111*, D24S01. https://doi.org/10.1029/2006JD007905

Skamarock, W. C., Klemp, J. B., Dudhia, J., Gill, D. O., Barker, D. M., Duda, M. G., … Powers, J. G. (2008). A description of the advanced research WRF version 3. Technical Report, (June), 113.

Stohl, A., Eckhardt, S., Forster, C., James, P., & Spichtinger, N. (2002). On the pathways and timescales of intercontinental air pollution transport. *Journal of Geophysical Research*, *107*(D23), 4684. https://doi.org/10.1029/2001JD001396

Thouret, V., Cammas, J.-P., Sauvage, B., Athier, G., Zbinden, R., Nédélec, P., … Karcher, F. (2005). Tropopause referenced ozone climatology and inter-annual variability (1994–2003) from the MOZAIC programme. *Atmospheric Chemistry and Physics*, *6*, 1033–1051.

U.S. Environmental Protection Agency (2007). 2005 National Emission Inventory. Retrieved from https://www3.epa.gov/ttnchie1/net/2005inventory.html

Vennam, L. P. (2016). Assessment of aircraft emissions impacts on air quality at multiple model scales, Chapter 4. (Doctoral dissertation, The University of North Carolina at Chapel Hill).

Vennam, L. P., Arunachalam, S., Baek, B. H., Omary, M., Binkowski, F., & Mathur, R. (2013). A tracer study to assess transport of cruise altitude aircraft emissions to the surface at continental and hemispheric scales. In Proceedings of the 12th Annual CMAS Conference, Chapel Hill, NC, Oct 2013.

Vennam, L. P., Arunachalam, S., Baek, B. H., Omary, M., Binkowski, F., Olsen, S., … Fleming, G. (2014). *A Multiscale Modeling Study to Assess Impacts of Full-Flight Aircraft Emissions on Upper Troposphere and Surface Air Quality. Air Pollution Modeling and its Application XXIII* (pp. 197–203). Switzerland: Springer International Publishing.

Waitz, I. A., Lukachko, S. P., & Lee, J. J. (2005). Military aviation and the environment: Historical trends and comparison to civil aviation. *Journal of Aircraft*, *42*, 329–339. https://doi.org/10.2514/1.6888

Wauben, W. M. F., Velthoven, P. F. J. V., & Kelder, H. (1997). A 3D chemistry transport model study of changes in atmospheric ozone due to aircraft NO_x emissions. *Atmospheric Environment*, *31*(12), 1819–1836. https://doi.org/10.1016/S1352-2310(96)00332-9

Wayson, R. L., Fleming, G. G., & Iovinelli, R. (2009). Methodology to estimate particulate matter emissions from certified commercial aircraft engines. *Journal of the Air & Waste Management Association*, *59*, 91–100. https://doi.org/10.3155/1047-3289.59.1.91

West, J. J., Naik, V., Horowitz, L. W., & Fiore, A. M. (2009). Effect of regional precursor emission controls on long-range ozone transport—Part 2: Steady-state changes in ozone air quality and impacts on human mortality. *Atmospheric Chemistry and Physics*, *9*, 6095–6107. https://doi.org/10.5194/acp-9-6095-2009

Whitt, D. B., Jacobson, M. Z., Wilkerson, J. T., Naiman, A. D., & Lele, S. K. (2011). Vertical mixing of commercial aviation emissions from cruise altitude to the surface. *Journal of Geophysical Research*, *116*, D14109. https://doi.org/10.1029/2010JD015532

Whitten, G. Z., Heo, G., Kimura, Y., McDonald-Buller, E., Allen, D. T., Carter, W. P. L., & Yarwood, G. (2010). A new condensed toluene mechanism for carbon bond: CB05-TU. *Atmospheric Environment*, *44*, 5346–5355. https://doi.org/10.1016/j.atmosenv.2009.12.029

Wilkerson, J. T., Jacobson, M. Z., Malwitz, A., Balasubramanian, S., Wayson, R., Fleming, G., … Lele, S. K. (2010). Analysis of emission data from global commercial aviation: 2004 and 2006. *Atmospheric Chemistry and Physics*, *10*, 6391–6408. https://doi.org/10.5194/acp-10-6391-2010

Woody, M., Haeng Baek, B., Adelman, Z., Omary, M., Fat Lam, Y., Jason West, J., & Arunachalam, S. (2011). An assessment of Aviation's contribution to current and future fine particulate matter in the United States. *Atmospheric Environment*, *45*, 3424–3433. https://doi.org/10.1016/j.atmosenv.2011.03.041

Woody, M. C., West, J. J., Jathar, S. H., Robinson, A. L., & Arunachalam, S. (2015). Estimates of non-traditional secondary organic aerosols from aircraft SVOC and IVOC emissions using CMAQ. *Atmospheric Chemistry and Physics*, *15*(12), 6929–6942. https://doi.org/10.5194/acp-15-6929-2015

Xing, J., Mathur, R., Pleim, J., Hogrefe, C., Gan, C.-M., Wong, D. C., … Pouliot, G. (2015). Observations and modeling of air quality trends over 1990–2010 across the Northern Hemisphere: China, the United States and Europe. *Atmospheric Chemistry and Physics*, *15*(5), 2723–2747. https://doi.org/10.5194/acp-15-2723-2015

Xing, J., Mathur, R., Pleim, J., Hogrefe, C., Wang, J., Gan, C.-M., … McKeen, S. (2016). Representing the effects of stratosphere-troposphere exchange on 3-D O_3 distributions in chemistry transport models using a potential vorticity based parameterization. *Atmospheric Chemistry and Physics*, *16*(17), 10,865–10,877. https://doi.org/10.5194/acp-16-10865-2016

Yan, Y., Lin, J., Chen, J., & Hu, L. (2016). Improved simulation of tropospheric ozone by a global-multi-regional two-way coupling model system. *Atmospheric Chemistry and Physics*, *16*(4), 2381–2400. https://doi.org/10.5194/acp-16-2381-2016

Yang, H., Chen, G., Tang, Q., & Hess, P. (2016). Quantifying isentropic stratosphere-troposphere exchange of ozone. *Journal of Geophysical Research: Atmospheres*, *121*, 3372–3387. https://doi.org/10.1002/2015JD024180

Yim, S. H. L., Lee, G. L., Lee, I. H., Allroggen, F., Ashok, A., Caiazzo, F., … Barrett, S. R. H. (2015). Global, regional and local health impacts of civil aviation emissions. *Environmental Research Letters*, *10*(3), 34001. https://doi.org/10.1088/1748-9326/10/3/034001

Zyryanov, D., Foret, G., Eremenko, M., Beekmann, M., Cammas, J. P., D'Isidoro, M., … Flaud, J. M. (2012). 3-D evaluation of tropospheric ozone simulations by an ensemble of regional chemistry transport model. *Atmospheric Chemistry and Physics*, *12*, 3219–3240. https://doi.org/10.5194/acp-12-3219-2012